Lineage commitment pathways epigenetically oppose oncogenic Gαq/11-YAP signaling in dormant disseminated uveal melanoma.

Rama Kadamb[1], Melisa Lopez Anton[2,3], Timothy J. Purwin[4], Vivian Chua[4,#5], Lornella Seeneevassen[1], Jessica Teh[4], M. Angela Nieto[3], Takami Sato[6], Mizue Terai[6], Sergio Roman Roman[7], Leanne De Koning[7], Deyou Zheng[8], Andrew E Aplin[4] and Julio Aguirre-Ghiso[1,9,10,11,12,*]

[1]Department of Cell Biology, Montefiore Einstein Comprehensive Cancer Center, Albert Einstein College of Medicine, Bronx, NY, USA.
[2]Division of Hematology and Oncology, Department of Medicine, The Tisch Cancer Institute, Icahn School of Medicine at Mount Sinai, New York, NY.
[3] Instituto de Neurociencias (CSIC-UMH) and CIBERER, Alicante, Spain.
[4]Department of Pharmacology, Physiology, and Cancer Biology and the Sidney Kimmel Cancer Center, Thomas Jefferson University, Philadelphia, PA 19107, USA.
[#5]School of Medical and Health Sciences, Edith Cowan University, Joondalup, WA 6027, Australia. Centre for Precision Health, Edith Cowan University, Joondalup, WA 6027, Australia
[6] Department of Medical Oncology, Thomas Jefferson University, Philadelphia, PA.
[7]Department of Translational Research, Institut Curie, PSL Research University, Paris, F-75005, France.
[8] Departments of Genetics, Neurology and Neuroscience, Albert Einstein College of Medicine, Bronx, NY, USA.
[9]Cancer Dormancy and Tumor Microenvironment Institute, Montefiore Einstein Comprehensive Cancer Center, Albert Einstein College of Medicine, Bronx, NY, USA.
[10]Gruss-Lipper Biophotonics Center, Albert Einstein College of Medicine, Bronx, NY, USA.
[11]Ruth L. and David S. Gottesman Institute for Stem Cell Research and Regenerative Medicine, Albert Einstein College of Medicine, Bronx, NY, USA
[12]Institute for Aging Research, Albert Einstein College of Medicine, Bronx, NY, USA

*Correspondence: julio.aguirre-ghiso@einsteinmed.edu
[#] Present affiliation

Keywords: Uveal melanoma, Dormancy, Metastasis, NR2F1, Histone modifications, Chromatin, Hippo pathway, H2B-GFP label retention.

Abbreviations: UM: Uveal melanoma; DCCs: Disseminated Cancer Cells; GPCR: G-protein coupled receptor; QR: Quiescence reporter.

Highlights:

- Quiescent solitary uveal melanoma (UM) DCCs in the liver up- and down-regulate neural crest and cell cycle progression programs, respectively.
- NR2F1 drives solitary UM DCC dormancy by antagonizing the Gαq/11-YAP1 pathway; small molecule Gαq/11 inhibition restores NR2F1 expression and quiescence.
- NR2F1 short-circuits oncogenic YAP1 and G-protein signaling *via* a chromatin remodeling program.
- Loss of function of NR2F1 in dormant UM DCCs leads to aggressive liver metastasis.

Abstract

The mechanisms driving late relapse in uveal melanoma (UM) patients remains a medical mystery and major challenge. Clinically it is inferred that UM disseminated cancer cells (DCCs) persist asymptomatic for years-to-decades mainly in the liver before they manifest as symptomatic metastasis. Here we reveal using Gαq/11^{mut}/BAP^{wt} human uveal melanoma models and human UM metastatic samples, that the neural crest lineage commitment nuclear receptor NR2F1 is a key regulator of spontaneous UM DCC dormancy in the liver. Using a quiescence reporter, RNA-seq and multiplex imaging we revealed that rare dormant UM DCCs upregulate NR2F1 expression and genes related to neural crest programs while repressing gene related to cell cycle progression. Gain and loss of function assays showed that NR2F1 silences YAP1/TEAD1 transcription downstream of Gαq/11 signaling and that NR2F1 expression can also be repressed by YAP1. YAP1 expression is repressed by NR2F1 binding to its promoter and changing the histone H3 tail activation marks to repress YAP1 transcription. *In vivo* CRISPR KO of NR2F1 led dormant UM DCCs to awaken and initiate relentless liver metastatic growth. Cut&Run and bulk RNA sequencing further confirmed that NR2F1 epigenetically stimulates neuron axon guidance and neural lineage programs, and it globally represses gene expression linked to G-protein signaling to drive dormancy. Pharmacological inhibition of Gαq/11^{mut} signaling resulted in NR2F1 upregulation and robust UM growth arrest, which was also achieved using a novel NR2F1 agonist. Our work sheds light on the molecular underpinnings of UM dormancy revealing that transcriptional programs driven by NR2F1 epigenetically short-circuit Gαq/11 signaling to its downstream target YAP1.

Introduction

At the time of diagnosis, less than 5% of uveal melanoma (UM) patients have evidence of metastasis. However, up to 50% of UM patients will ultimately succumb to advanced metastatic disease [1,2]. The liver is the predominant organ of metastasis [3,4] and standard chemotherapies rarely induce clinical responses in patients with macro-metastasis [5–7] and patient 1-year survival is 30-50% [8,9]. A few drugs have been shown (e.g., tebentafusp and melphalan) to provide benefit in metastatic uveal melanoma [10,11] but they only increase overall survival by few months. Thus, preventing the occurrence of metastatic disease remains an urgent unmet need for effective therapeutic strategies for UM.

Risk of metastatic disease and UM associated survival is strongly correlated with mutation in key proteins [12,13]. Activating mutations (typically Q209) in alpha subunits of the heterotrimeric G proteins, *GNAQ* and *GNA11* were the first described driver mutations in UM and are found in 80-94% of UM [14–17]. Mutation of the genes, *SF3B1* and *EIF1AX*, are associated with a favorable prognosis [17,18]. Monosomy of chromosome 3 is associated with poor prognosis [19]. Inactivating mutations of *BAP1* (BRCA1-associated protein 1) on 3p21.1 are found in 32-50% of primary uveal melanomas [20–22] and associate with a higher likelihood of metastasis [23,24]. *BAP1* encodes a de-ubiquitinating enzyme that removes mono-ubiquitin from histone H2A leading to activation of gene transcription [25,26]. BAP1 is also implicated in DNA repair, cell cycle progression and cell differentiation [27–29]. Furthermore, high expression of PRAME (preferentially expressed antigen in melanoma) is associated with metastasis [30]. The roles of BAP1 loss and elevated PRAME levels in UM remain to be understood. It is also evident from clonal phylogenetic analysis and autopsy studies that in a significant proportion of patients, UM can disseminate very early in evolution [31–33] and colonize multiple sites, with the liver being the site with highest frequency of seeding. Thus, UM dissemination is systemic, and UM disseminated cancer cells (DCCs) could remain inactive or dormant and undetected for long periods in the liver and other sites.

A long-standing question in UM is the mechanisms that allows uveal melanoma cancer cells to display a remarkable delayed time to metastasis, a phenomenon already recognized before the early 60's with case reports dating back to the 40s'and earlier [34], but the mechanisms have remained unknown. How UM DCCs persist in this dormant form for so long, particularly in the liver, is a key clinical problem. Metastases often take years-to-decades to grow out and do so without recurrence at the primary site, highlighting early dissemination and tumor cell dormancy at distant sites as reported for UM and other cancers [33,35–37]. UM liver dormancy is supported by studies in which fluorescently labeled cells were tail vein-injected into mice and non-proliferative single cells were identified in the liver [38]. However, the mechanisms underlying delayed relapse and why the liver is a preferred site for survival and eventual regrowth remained unknown.

Melanocytes in the eye are derived from neural crest cells [39,40]. We identified lineage commitment transcription factors (TFs) such as DEC2/BHLHE41 in the muscle and NR2F1 in neural crest cells, and primed pluripotency regulators like ZFP281 in the blastocyst are key regulators of dormancy in various cancer models [41–43]. Interestingly NR2F1 is specifically involved in lineage commitment of neural crest cells and differentiation during eye development [44,45]. The above mentioned TFs are regulated by upstream autocrine or niche-derived signals such as retinoic acid, TGFβ2, BMP7 and WNT5a. Downstream TFs such as NR2F1 and ZFP281 induce quiescence by upregulating a repressive chromatin state and cyclin-dependent kinase (CDK) inhibitor (e.g., $p27^{Kip1}$,p16) and by blocking G1-S transcriptional programs [42,46]. In cutaneous melanoma a dormant phenotype is associated with phenotype switching linked to activation of neural and mesenchymal programs that cause growth arrest. Further, therapy-induced residual "persister" disease in cutaneous melanoma was also linked to adaptive transcriptomic changes and epigenetic remodeling [47]. Whether similar mechanisms are also operational in UM dormancy was unknown until now.

Here we reveal, using xenotransplantation and unbiased isolation of quiescent human UM DCCs from the liver, that in Gαq/11^{mut}/BAP^{wt} human uveal melanoma cells, NR2F1 is a key regulator of dormancy of DCCs. Mechanism analysis revealed that dormant UM DCCs upregulate NR2F1 expression while silencing YAP/TEAD transcription and growth programs. NR2F1 and YAP1 mutually antagonize their expression and NR2F1 binding to the YAP1 promoter that displays a loss of histone H3 activation marks and thus short-circuits oncogene signaling. Importantly, agonist mediated NR2F1 activation or targeted inhibition of Gαq/11^{mut} enhances NR2F1 expression, blocking growth. UM solitary DCCs in mice and humans upregulated NR2F1 and *in vivo* CRISPR KO of NR2F1 results in dormant DCC awakening and massive liver metastatic disease. Our research provides explanation to the long-held mystery of uveal melanoma dormancy. Additionally, it broadens the paradigm which shows the way through which dormancy pathways can be strong enforcers of growth arrest programs that can epigenetically override apparently irreversible oncogenic programs caused by driver mutations.

Results

Long-lived dormancy of human UM DCCs in mouse livers.

Clinical experience suggest that disseminated UM cells persist in livers for very long periods and that even as metastatic lesions they are slow proliferating [30,48,49]. To model this behavior in mice we engineered human Gαq/11^{mut} OMM1.3 UM cells to dually express H2B-GFP from an inducible TET-ON promoter and Td-Tomato from a constitutive promoter (OMM1.3-QR, for OMM1.3 **q**uiescence **r**eporter line) (**Fig. 1A**). The H2B-GFP inducible system was used to label nucleosomes that could then be chased for label retention analysis as reported for tracking quiescent hematopoietic stem cells for the life of the mouse [50]. OMM1.3 cells that proliferate dilute the H2B-GFP signal and eventually are detected as H2B-GFP$^-$/Td-Tomato$^+$ (OMM1.3-QR$^-$ cells). In contrast, OMM1.3 cells that remain non-proliferative persist as H2B-GFP$^+$/Td-Tomato$^+$ cells (OMM1.3-QR$^+$ cells) (**Fig. 1A**). Doxycycline-pulsed OMM1.3-QR$^+$ cells were injected into the spleens of nude mice, which allows for efficient spontaneous seeding of the liver [51]. Then these animals were monitored for 1, 3 and 4 months for any signs of disease progression **(Fig. 1B)**. Monitoring of OMM1.3-QR cells in the liver using FACS for population analysis, revealed that at 1 month ~80% OMM1.3-QR cells are dually labeled and thus quiescent (**Fig. 1C; Fig. S1.1**). At 3 months the livers still contained ~55% OMM1.3-QR$^+$ quiescent cells vs. ~45% OMM1.3-QR$^-$ cells (**Fig. 1C and Fig. S1.1).** At 4 months the livers still carried ~5% of OMM1.3-QR$^+$ cells, while more than 95% were proliferative **(Fig. 1C; Fig. S1.1**). Monitoring of OMM1.3-QR cells in livers at 3-month using epifluorescence microscopy, revealed that both solitary QR+ DCCs (GFP$^+$ cells) and larger QR- micro-metastasis population existed and can be seen located outside or also within sinusoids (black in green liver autofluorescence background) and (**Fig. 1D**). Inspection of the spleens at those time points revealed no visible UM growth but occasional solitary DCCs remained (**data not shown**). We conclude that upon arrival in the liver the predominant phenotype of human UM DCCs is a non- or slow-proliferative state. Importantly, the data at 3 and 4 months (between 9-12 years in humans) suggest that dormant cells persist and co-exist with proliferative lesions in the same organ for very long periods.

Culturing Dox induced OMM1.3-QR cells as solitary cells at low density in 3D organoid cultures revealed that, as in the livers, these cells are also inherently cycling slowly with ~25 and ~18% of label retaining cells persisting at 7- and 14-days post seeding, respectively **(Fig. S1A)**. Together our data reveal that OMM1.3 can recapitulate, *in vitro* and *in vivo,* a slow cycling or deep dormant phenotype of UM DCC and allow its study.

Differential regulation of neural and cell cycle programs in quiescent vs. proliferative UM DCCs.

OMM1.3-QR$^+$ or OMM1.3-QR$^-$ cells were isolated from mouse livers via FACS at 1, 2, and 3 months and RNA-seq was carried out. These time points were selected to increase the chance of

detecting quiescent cells (**Fig S1.1A-C)**. Analysis of the RNA-seq data reads of OMM1.3-QR$^+$ UM DCCs after 1- and 2-months revealed very low level of human cells and the RNA-seq data was unreliable, possibly due to low numbers of cells recovered from the livers and/or contamination with host cells despite careful sorting. However, at 3 months we isolated sufficient number of QR$^+$ and QR$^-$ tagged cells from three animal mouse livers (n=3) to provide interpretable abundant RNA-seq data **(Fig. S1.1D)**. We also collected cultured OMM1.3 cells as a continuous proliferative control **(Fig. S1.1E)**. The RNA-seq reads were analyzed to reflect gene expression in OMM1.3-QR$^+$ over OMM1.3-QR$^-$ cells. Unbiased clustering by the number of expressed genes revealed that all three OMM1.3-QR+ samples clustered away from the RNA samples of OMM1.3-QR$^-$ cells; these cells also clustered closer to the proliferative *in vitro* culture OMM1.3 supporting the notion that metastatic reactivation programs match the basic UM proliferative pathways (**Fig. S1B**). Further, differentially expressed gene (DEG) analysis from RNA-seq revealed that the majority of DEGs in OMM1.3-QR$^+$ cells were downregulated (3356 genes, ~90% of DEGs), suggesting a strong decrease in cellular processes during the 3-month dormancy **(Fig. 1E and Fig. S1C)**. Accordingly, pathways analysis from genes downregulated in OMM1.3-QR$^+$ UM DCCs using Enrichr database revealed that genes associated with regulation of transcription, cell cycle progression, RNA Pol II transcription, mitotic spindle organization and regulation of cyclin/CDK complexes microtubule regulation, involved in mitosis as well as pathways related to positive upregulation of GTPase activity were significantly downregulated (**Fig. 1F and Table S1A**).

The pathways associated with the downregulated genes (**Fig. 1F-H,** 311, ~10% of all DEGs) in dormant UM population show more than -6 $\log_2$ FC of key cell cycle regulatory genes confirming a growth arrest program in these cells (**Fig. S1D**). Among the upregulated genes, we found an upregulation of mRNA catabolic processing and protein targeting to the ER reminiscent of ER stress program in dormant UM DCCs that has been reported previously in dormant cancer cells **(Fig. 1G & Table S1B)** [52,53]. We further analyzed pathways by using only 100 most upregulated and most downregulated genes based on $\log_2$ fold change in either direction in dormant UM DCCs and found that pathways suppressing G2/M transition of cell cycle and small GTPase activity were downregulated in dormant UM DCCs **(Fig. S1E)**. In contrast, pathways related to negative regulation of transcription and positive regulation of differentiation of neuronal lineage committed progenitors were upregulated **(Fig. S1F)**. Intriguingly, we found genes linked to neural fate regulation, neurotransmitter signaling, and neurological disorders were indeed upregulated and cell cycle and transcriptional regulatory genes are downregulated (**Fig. 1H)**. Since uveal melanocytes are derived from neural crest cells, further, selective analysis of a neural crest cell signature activated in dormant UM DCCs population revealed a strong induction of these genes in OMM1.3-QR+ cells (**Fig. 2A**). This led us to hypothesize that proliferative OMM1.3 cells are in a de-differentiated state and when entering dormancy as OMM1.3-QR$^+$ cells they upregulate neural lineage commitment genes. Owing to role of NR2F1 in regulation of both melanocytic lineage and in maintaining dormancy, we looked at the expression of NR2F1 in OMM1.3-QR$^+$ and OMM1.3-QR$^-$ cell population. We did not detect NR2F1 expression in our RNA-seq analysis, possibly due to low transcript abundance from the rare OMM1.3-QR$^+$ cells. However, qRT-PCR from an independent experiment with newly sorted OMM1.3-QR$^+$ and OMM1.3-QR$^-$ UM cells at 3 months showed more than 5-fold upregulation of NR2F1 expression level compared to proliferative UM DCCs at 3-month time point (**Fig. 2B**). This observation was further strengthened by our in-vivo assay using high resolution confocal microscopy, where we found selective upregulation of NR2F1 in the nuclei of solitary UM DCCs and small clusters (dormant) vs. large clusters (proliferating cells) in the liver of mice, that were intrasplenicaly injected with either (UM004 or OMM1.3) (**Fig. 2C**). Importantly, we found that NR2F1 expression was inversely correlated with Ki67 expression in both UM004 and OMM1.3 cells (**Fig. S2A**). Data from RNA-seq and *in-vivo* experiments confirming slow proliferation as evident by downregulation of cell cycle genes and low staining for Ki67 were also recapitulated in our 3D model. We found that nuclei of slow proliferating OMM1.3 cells in 3D that generate either solitary UM cells or clusters smaller

than 8 cells were 100% positive for NR2F1 expression. In contrast, proliferative OMM1.3 UM cell clusters, larger than 8 cells (> 8-cells) showed significantly lower frequency of NR2F1 expression (**Fig. 2D**). These observations imply that UM cancer cells that enter quiescence upregulate lineage commitment programs associated with neural crest identity and strongly downregulate proliferation programs and might maintain dormant phenotype in UM cells.

Increased expression of NR2F1 in human UM solitary cells compared to proliferative/ metastatic masses co-existing in human livers.

Liver samples from UM patients before overt metastases that would potentially carry dormant DCCs are unavailable. However, we have shown in mouse models, including Fig. 1 and 2, and patient samples [54,55] that solitary or small cluster of DCCs can co-exist with larger metastatic lesions in the same organ and express dormancy markers. Given that NR2F1 is key regulator of dormancy program in several cancer models [42,56–58] and we observed that dormant UM population significantly enhance NR2F1 expression. This prompted us to test whether the association of increased NR2F1 in dormant DCCs also holds true in patients' UM liver metastatic samples by quantifying NR2F1 expression in solitary DCCs or isolated small clusters (surrounding near the metastatic lesion or farther away in the normal liver tissue), metastatic lesion edge and core of metastatic lesion. For this, patient's samples were immunostained for NR2F1; HMB45 was used to track the UM cells. Immunofluorescence analysis on these patient samples revealed that like in the xenograft models, HMB45$^+$ solitary and small clusters of UM DCCs had more frequently upregulated NR2F1 protein **(Fig. 2E)**. Interestingly we also found that hepatocytes also express NR2F1 **(Fig. 2C&E)**. UM cells at the edge of the metastatic lesions (cancer/stroma interface), where cancer cells interact more closely with the liver tissue, had also upregulated NR2F1 (**Fig. 2E; Metastatic edge panel).** The opposite was true for the core of the proliferative metastasis; these cells had completely downregulated NR2F1 expression as can be seen in the images and by quantification of mean NR2F1 intensity (**Fig. 2E; metastatic core panel)**. Overall, all analyzed patient samples showed that NR2F1 intensity is higher in solitary/isolated clusters compared to large clusters (includes metastatic edge/core) **(Fig. S2B)**. In conclusion, NR2F1 is detected efficiently in UM samples and its upregulation correlates with the solitary and small cluster state as well as with the interaction of UM cells with the liver microenvironment. In contrast, proliferative lesions either downregulate NR2F1 expression or completely abolish its expression.

YAP and NR2F1 gene expression is inversely regulated in dormant UM DCCs.

Our data support the idea that NR2F1 and neural crest-related genes are upregulated in OMM1.3-QR$^+$ cells, while concomitantly displaying downregulated proliferation programs (**Fig. 1-2**). In UM with the Gαq/11 driver mutations the mutant is known to upregulate YAP/TAZ/TEADs pathway [59]. RNA-seq data revealed that compared to proliferating QR$^-$ UM DCCs cells, in the quiescent OMM1.3-QR$^+$ cells several TFs (e.g., YAP1, TEAD1, TEAD3 – **Fig. 3A**) and their target genes (e.g., NUAK2, DOC5) of the YAP pathway were significantly downregulated. Interestingly, the *Wnt* related pathway was also downregulated in the OMM1.3QR$^+$cells (**Fig. 3A)**. The downregulation of YAP1 mRNA in OMM1.3-QR$^+$ cells as compared to QR$^-$ cells isolated from mouse livers after 3 months of growth was further confirmed by qRT-PCR **(Fig. 3B)**. We next tested whether, as in **Fig. 2D**, if there was a difference in YAP1 expression in small vs. large proliferative UM cell clusters. We found that while solitary cells were negative for YAP1, those which had clusters consisting of >2 cells, had significantly upregulated YAP1 **(Fig. 3C)**.

To pinpoint the role of NR2F1 in maintenance of the dormant (single cell) state of UM, we performed transient knockdown of NR2F1. In 3D cultures RNAi targeting of NR2F1 resulted in accelerated growth of OMM1.3 cells as revealed by a reduced ratio of OMM1.3-QR+ to QR- cells and increased frequency of large UM cell cluster, arguing that *NR2F1* loss accelerated UM proliferation (**Fig. 3D-F**). YAP1, TEAD1 and

TEAD2 expressions were upregulated upon RNAi-mediated knock down of NR2F1 in these cells. Although, expression of TAZ and TEAD3 genes remains unchanged upon transient knockdown of NR2F1 (**Fig. 3G**) downstream target genes ANKRD1, CTGF1 and CYR61 showed significant upregulation upon knockdown of NR2F1 (**Fig. S3A**). In accordance with previous report that YAP1 promotes growth and tumor progression of UM cells, we found that transient knockdown of YAP1 resulted in profound reduction in proliferative cell clusters and in growth suppression of UM cells in 3D culture (**Fig. 3H**). Interestingly, YAP1 was found to negatively regulate NR2F1 expression as RNAi targeting of YAP1 resulted in increased mRNA and protein levels of NR2F1 (**Fig. 3I and Fig. S3B)**. Moreover, NR2F1 was found to negatively regulate YAP1 mRNA expression; when induced with DOX in UM004 cells (also Gαq/11^{mut}/BAP^{wt}), it forced the cells to enter the NR2F1+ solitary DCC state, while downregulating YAP1 and its co-activator TEAD1 expression at protein level (**Fig. 3J and Fig. S3C**). Inducible expression of NR2F1 in UM004 cells also strongly suppressed the ability of solitary UM cancer cells to transition into proliferative cell clusters (**Fig. 3K**). Further, we found that constitutive presence of NR2F1 is required to maintain growth suppression as removal of doxycycline from culture medium de-represses the growth inhibitory signal and enables the single cell to proliferate into big clusters (**Fig. S3D-E**). As shown for knockdown of NR2F1 in OMM1.3 cells where it caused activation of YAP1 and its co-activator genes complex, TEADs at protein level **(Fig. 3L)** NR2F1 knockdown in UM004 cell also led to upregulation of YAP1 mRNA but without significant changes in TEAD1 and TEAD3 (**Fig. S3F**). The findings in OMM1.3 cells where NR2F1 knockdown and upregulation of YAP1 was accompanied by accelerated growth of cells in 3D as evident by increase in cluster colonies, were recapitulated in UM004 cells (**Fig. 3M**) suggesting it is not an OMM1.3-specific finding.

Finally, to determine whether this apparent mutually antagonistic regulation between NR2F1 and YAP1 was part of the biological makeup of UM, we stained liver sections recovered from mice injected intra-splenically with UM004 cells and patient samples with liver metastases for co-detection of these two TFs (antibody species prevented co-detection). The data revealed that there was a strong inverse correlation between NR2F1 and YAP1 in solitary/small, isolated clusters of UM DCCs and growing metastatic lesions in mouse liver (**Fig. 3N**). Antagonism between YAP1 and NR2F1 levels was further confirmed in metastatic UM patient sample. Our data revealed a very strong inverse relationship between NR2F1 and YAP1 expression profile in solitary/isolated small clusters vs. large clusters (coming from either metastatic core or edge area) **(Fig. 3O).** Overall, our data supports the idea that NR2F1 acts as an antagonist of the YAP pathway downstream of oncogenic Gαq/11 signaling and that it can suppress UM awakening and proliferation.

Assembly of YAP1-TEAD1 complex is negatively regulated by NR2F1.

UM progression is heavily influenced by YAP1 and our observations from Figure 3 indicate that NR2F1 negatively regulates YAP1. This led us to further explore the mechanism and significance of the negative regulation of YAP1 by NR2F1. To this end we generated two independent NR2F1 CRISPR knock out OMM1.3 lines. Successful knockout of NR2F1 (NR2F1_KO1 & NR2F1_KO2) was confirmed by western blot and immunofluorescence (**Fig. 4A& Fig. S4A**). Specificity of CRISPR knockout was further confirmed by immunoblotting NR2F2 (isoform of NR2F1) that remains unchanged by CRISPR mediated knockout (**Fig. 4SB**). NR2F1 KO resulted in significant upregulation of YAP1, TEAD1 (**Fig. 4A**) along with mild upregulation of TAZ (**Fig. 4SB**). YAP1 upregulation is also accompanied by upregulation of its prototypical target gene, CTGF1 (**Fig. 4B**). Interestingly, the master regulator of the melanocyte lineage transcription factor (MITF1) was also upregulated upon NR2F1 KO suggesting a potential role for NR2F1 in controlling lineage switching when negatively regulating YAP1 expression and function (**Fig. 4B**). The phosphorylation of ERK1/2 (p-ERK1/2) was also increased upon NR2F1 KO arguing that the Gαq/11-ERK1/2-YAP signaling axis is being restored upon NR2F1 loss (**Fig. 4B**). In contrast, gain of function experiments in UM004 cells with an inducible NR2F1 under dox control led to downregulation of YAP1

(shown in Fig. 3J and Fig. 4SB), CTGF1, MITF and p-ERK1/2; even TAZ appeared downregulated when NR2F1 was strongly upregulated (**Fig. 4B & Fig. 4SB**). Some target genes showed better dose dependence to NR2F1 induction than others suggesting a dynamic regulation of the growth suppressive effect by NR2F1.

We next tested if the effect of YAP1 downregulation caused by NR2F1 was, via a mass effect, sufficient to reduce the assembly of the YAP1/TEAD1 complexes required for efficient transcriptional activity. Indeed, NR2F1 KO in OMM1.3 cells resulted in increased interaction between YAP1 and its co-activator TEAD1 as determined by co-immunoprecipitation (Co-IP) analysis (**Fig. 4C**). This increased interaction is specific to YAP-TEAD1 as we found that YAP1 interaction with LATS1 remains unaffected upon NR2F1 deletion (**Fig. 4SC**). We next used the gain of function approach in UM004 cells with the Dox inducible system to induce NR2F1 expression. These results confirmed that NR2F1 upregulation reduces expression of YAP1 and TEAD1 and, consequently their interaction, as shown by Co-IP (**Fig. 4D**), greatly reduces the transcriptional complex formed by these two TFs.

Based on these data, we propose that loss of NR2F1 in UM cells should unleash an unrestricted growth program driven by YAP1 signaling downstream of Gαq/11 signaling. To test this hypothesis, we first grew WT-NR2F1 and KO-NR2F1 OMM1.3 cells in organoid media to determine their "stem-like" capacity and how it is influenced by NR2F1 loss. These results showed that the KO of NR2F1 stimulated growth of larger colonies by UM cells (**Fig. 4E**). We next tested whether this ability for enhanced growth would be able to interrupt the long lasting (months) dormant state of OMM1.3 cells in the mouse livers (**Fig. 1**). To test this hypothesis, we injected WT-NR2F1 and KO-NR2F1 OMM1.3 cells via intrasplenic injection into nude mice and 3 months later solitary DCCs, micro- and macro-metastasis were scored by visual inspection of the livers and via histological and immunofluorescence analysis (**Fig. 4F-G**). Our data show that WT-NR2F1 OMM1.3 cells were for the most part unable to form visible metastasis and IF analysis using human specific vimentin to track UM cells showed the perivascular persistence of solitary UM DCCs at 3 months **(Fig. 4F-G)**. In contrast, KO-NR2F1 OMM1.3 cells were able to overcome all growth restrictions and formed metastatic lesions that invaded large sections of the liver, and this was true for both KO-NR2F1 OMM1.3 cell lines (**Fig. 4F-G**). We next assessed whether NR2F1 deletion affects the number of UM cells that reach the liver after intrasplenic injection and found that NR2F1 KO does not increase the number of cells seeded in the liver. Hence the massive metastatic burden observed in the livers seeded with the NR2F1 suppressed cells must be the result of re-activation of the dormant UM DCCs (**Fig. 4SD**). Moreover, staining of liver sections from NR2F1 KO mice showed that YAP1 is barely expressed in solitary cells/small clusters in control mice group while it is abundantly expressed in large NR2F1 KO metastatic lesions (**Fig. 4H**) confirming that loss of NR2F1 allows the oncogenic program to override the dormancy program. We conclude that by dismantling YAP1/TEAD1 complex NR2F1 upregulation imposes on UM DCCs a dormancy program that impedes metastasis.

NR2F1 represses YAP1 gene transcription via histone H3 modifications and inhibits GPCR-linked gene expression.

Our results showing the apparent invert interdependence between NR2F1 and YAP1 mRNA levels suggest a plausible transcriptional repression mechanism induced by NR2F1 to silence YAP1 transcription. In-silico analysis confirms that YAP1 promoter has putative binding sites for NR2F1 that we confirmed in OMM1.3 cells. Using Chromatin precipitation (ChIP) assay, we found a significant enrichment of NR2F1 in upstream region of TSS (around -320bp to -1000bp) near YAP1 promoter region (**Fig 5A-B**). Further analysis using qPCR revealed that upon NR2F1 KO, the YAP1 gene showed an enrichment in H3K4me3, H3K27Ac activation marks but not H3K9me3 repressive mark on histone H3 at promoter sites (**Fig5C**). Using Dox-induction of NR2F1 in UM004 cell line, we observed NR2F1 enrichment on the YAP1 promoter with concomitant reduction in the active marks H3K4me3 and H3K27Ac accumulation but with no change in the repressive mark, H3K9me3 (**Fig. 5D)**. This suggests that

NR2F1 represses the activation of YAP1 transcription by possibly recruiting H3K4me3 demethylases and H3K27Ac deacetylases.

Having established that NR2F1 is repressing the transcription of YAP1, we then carried out a bulk RNA-seq to assess the transcriptional program regulated by NR2F1 under basal conditions in OMM1.3 cells. This observation is crucial because it appears that NR2F1 regulated program renders these cells dormant in the liver and is responsible for slow proliferation of these cells in 3D assays. It seems plausible, therefore, that NR2F1 governed gene expression program can provide clues to the establishment and facilitation of the dormancy phase. To gain insight into the scope of genes regulated by NR2F1 in OMM1.3 cells we carried out RNA-seq analysis in NR2F1 KO and WT OMM1.3 cells cultured in 3D assays. A Volcano plot (**Fig. 5E**) revealed a significant number of gene expression changes. Further analysis of these data revealed that in dormant UM cells NR2F1 is indeed positively regulating gene expression processes related to regulation of transcription, motor neuron axon guidance, axonogenesis, ganglioside biosynthetic pathways, mesenchymal cell migration, neural crest cell migration and neuron projection guidance **(Fig. 5F&G and Table S2A**). Some of these pathways included upregulation of RADIL, SOX9, PLX3A, PAK3, SLIT2 and SALL1 genes which are related to neural crest and axon guidance mechanisms. We also found that upon KO of NR2F1, NUP210 gene, which has been linked to metastasis initiation, was upregulated [60]. Interestingly, genes linked to cancer and metastasis such as SFRP1 and PPAR-γ were upregulated upon NR2F1 KD, suggesting that NR2F1 downregulation may allow their expression and function as reported by others [61] and us (**Fig. 5F**). Further, NR2F1 repressed biological processes that are involved in cell proliferation, angiogenesis and genes related to protein modification **(Fig. 5F&H and Table S2B**). Intriguingly, our analysis revealed that among the profoundly NR2F1-repressed genes, was an activator of GPCR signaling, GNAO1 which is known to interact with members of the genes in the G protein signaling network required for proliferation (**Fig. 5E&F)**. Findings of RNA-seq were further confirmed by qRT-PCR which showed that upon NR2F1 KO GNAO1 transcript was upregulated. In contrast, induction of NR2F1 (UM004 dox inducible NR2F1 cells) significantly suppressed GNAO1 mRNA expression levels (**Fig. S5A&B**). Collectively, the analysis of gene expression regulation by NFR2F1 and the ChIP-qPCR experiments points to a multilayered program that NR2F1 regulates to play a major role in dormancy regulation.

NR2F1 drives chromatin remodeling changes to repress GPCR signaling that can reciprocally antagonize NR2F1 expression.

The findings presented in Figure 5 suggest that there appears to be a chromatin remodeling program under the regulation of NR2F1, aimed at interrupting Gαq/11 oncogenic signaling. To explore this hypothesis, we used Cleavage Under Targets and Release Using Nuclease (CUT&RUN) for analyzing enrichment of histone H3K27me3, H3K27ac and H3K4me3 modifications globally in NR2F1-WT or NR2F1-KO cells cultured in 3D assays for 7 days when the phenotypes become evident (**Fig. 6A-B**). The analysis did not find a large reorganization of chromatin modifications but revealed many chromatin regions with both increased (n=788) and decreased (n=635) H3K27me3 upon NR1F1 KO (**Fig. 6A & Fig.S6A**), with 57% of the changes located to promoters. Similarly, we also found 564 genomic regions with significant H3K27Ac change upon loss of NR2F1 (**Fig. 6B & Fig. S6B**), with 92% at promoter regions. Interestingly, the level of changes in H3K27Ac seem more pronounced than those in H3K27me3 (**Fig. 6B & Fig. S6B**); we were unable to capture significant peaks for H3K4me3 mark and therefore, this mark was not considered in the analysis.

We searched for enriched gene ontology terms associated with the genes targeted by the altered histone modifications and revealed that NR2F1 is repressing GPCR signaling associated with glutamate receptor signaling as well as muscarinic and GABA receptor pathways (**Fig. 6C and Table S3A**). Genes that are associated with increased recruitment of repressive mark following NR2F1 KO (e.g., GRM3, GRM8, RXFP1) are shown to promote metastasis in different cancers (**Fig. 6C**). Interestingly, the

pathways for the genes with active histone modifications also revealed a neural pathway linked to other synaptic signaling pathways of less clear implications to induction of a dormant DCC phenotype in UM **(Fig. 6D and Table S3B**). Transcriptional initiation and regulation pathways are activated upon NR2F1 deletion as shown by enrichment of H3K27ac mark on genes involved in regulation of these pathways **(Fig. 6SC and Table S3C**). On the other hand, loss of H3K27ac activation marks from genes involved in nervous system development, differentiation and positive regulation of biosynthetic process are downregulated upon NR2F1 KO **(Fig. 6SD and Table S3D)**. These findings align with our *in-vivo* RNA-seq data that showed downregulation of these pathways in dormant UM DCCs (OMM1.3-QR+ cells). As YAP1 is a downstream effector protein of GPCR signaling and we found YAP1 downregulation by NR2F1, we looked at the distribution of H3K27me3 and H3K27Ac peaks onto YAP1. We found that NR2F1 KO leads to removal of H3K27me3 distribution at several positions while intensity of H3K27ac peak was enhanced near the promoter region of YAP1 (**Fig. 6E**). What emerged from analyzing the pathways enriched in our RNA-seq and chromatin remodeling experiments, is that regulators of G-protein signaling are being significantly repressed by NR2F1 induced chromatin changes modulating transcriptional program.

The above findings and the data showing that YAP1 downregulation could result in NR2F1 upregulation and suppress colony proliferation led us to test whether direct inhibitors of the Gαq/11 activity could reduce UM proliferation and induce NR2F1. For this, OMM1.3 cells treated with the cyclic depsipeptide YM-254890, a Gαq/11 inhibitor, greatly reduced the ability of these cells to form colonies in 3D Matrigel cultures (**Fig. 6F**). Further, the frequency of cells positive for NR2F1 increased in a dose dependent manner upon YM-254890 treatment. In cell clusters of less than 8 cells 100 nM treatment was achieving maximal induction of NR2F1 in this population of cells. In contrast, in big clusters that presumably were already formed at the time the treatment was initiated, (clusters larger than 8 cells) the effect was less pronounced but still highly significant with 300 nM dose showing the strongest induction of NR2F1 (**Fig. 6G**). This argues that either small clusters or larger clusters may be responsive to Gαq/11 inhibition to restore NR2F1 expression and dormancy onset. Simultaneously, we stained parallel 3D cultures for YAP1 expression and found YM treated colonies express low YAP1 compared to DMSO control (**Fig. 6H**). These observations support our hypothesis of a reciprocal and antagonistic regulation occurring between NR2F1 and Gαq/11 signaling. To further test the pharmacological approach to induce UM DCC dormancy, we treated OMM1.3 cells with a novel NR2F1 agonist, C26. This resulted in increased expression of NR2F1 at both transcript and protein level and colony growth and colony size were reduced when OMM1.3 cells were treated continuously with 50mM of C26 for 07 days (**Fig. 6SE-H**). We conclude that like Gαq/11 signaling is executing the negative regulation of NR2F1 expression likely via YAP1 as shown in Figure 3.

Discussion

The mechanisms behind the development of UM liver macro-metastasis, more than a decade after primary tumor treatment are still unclear [62]. It has been thought for long that early dissemination and DCC dormancy might explain this long known but poorly explained phenomena. These facts informed our current study. We assumed that identifying the mechanism that keeps disseminated metastatic cells in a state of dormancy will aid in developing novel approaches to UM treatment.

Using our H2B-GFP Tet ON/OFF label retention model for UM DCC dormancy, we successfully revealed that human Gαq/11^{mut}/BAP^{wt} UM DCCs can enter a prolonged dormancy state as solitary DCCs in the mouse liver equivalent to 9-12 years in humans. Previous studies revealed that Gαq/11 triggers the activation of the Hippo-YAP pathway, which represents a major driver in uveal melanoma progression [59,63]. Analysis of transcriptional programs in our OMM1.3-QR^{+} dormant and OMM1.3-QR^{-} UM DCCs also revealed that upon entry into dormancy the UM cells depart from a YAP1^{hi}/TEAD^{hi} state and acquire traits of neural lineage. Acquisition of the neural lineage is accompanied by silencing cell cycle progression, melanocytic and DNA synthesis programs. These changes are likely in response to a

de-differentiation process from a melanocytic program towards a neural lineage, which is also positively regulated by NR2F1 during development [44].

YAP1 and TEADs have been characterized as targets of the Gαq/11 oncogenic signaling for UM growth [63,64]. Thus, from a therapeutics point of view, it is an important finding that they are naturally downregulated during spontaneous dormancy of UM cells (OMM1.3-QR$^+$ cells). Melanocytes that serve as precursor for nevi cells for uveal melanoma initiation originates from neural crest cells [65,66]. NR2F1 a nuclear receptor with only recently identified putative ligands (e.g., sphingolipids) [67], is a critical regulator of this lineage program and serve a pivotal role in cortical pattering during eye morphogenesis [44,68,69]. Our data identified that among neural crest lineage genes, OMM1.3-QR$^+$ dormant UM DCCs upregulate NR2F1 expression, previously linked to dormancy in breast, head and neck squamous, and prostate cancer DCC models [58,70]. This allowed functionally determining that solitary DCCs or small DCC clusters (<8 cells) that enter dormancy must acquire a YAP1^{lo}/TEAD^{lo}/NR2F1^{hi} program. Upregulation of NR2F1 could be detected in solitary or small clusters of OMM1.3-QR$^+$ UM cells growing in 3D Matrigel, suggesting that the density of the UM cell cluster can make UM cells permissive for signals that turn on NR2F1 expression and a dormant phenotype. This observation was important as it suggested that the basal expression of NR2F1, which seems to repress UM progression genes, renders these OMM1.3 cells sensitive to enter dormancy in the liver and slowly proliferating in 3D assays. Thus, the gene expression program it governs at the basal state may provide insights into how it facilitates the dormancy phase (see below). Upregulation of NR2F1 protein was also detected in solitary and isolated small clusters of UM cells and in UM cells near the metastasis-liver boundary in both xenografts and human samples. These data were intriguing as they show that even advanced disease carries the ability to upregulate NR2F1 mostly when small cluster of UM cells or the edges of the metastatic lesions are in contact with the liver microenvironment. The core of the metastasis was largely NR2F1 negative and anticorrelated with Ki67 detection. It is tempting to speculate that NR2F1 could serve as a marker for dormancy of UM DCCs or in metastasis resected as a treatment option [42,56–58].

The inverse expression of mainly YAP1 and NR2F1 led us to explore how these TFs might be interconnected at a regulatory level. First, we determined the importance of NR2F1 in enabling a dormant phenotype as in 3D culture models, "melanosphere" cultures and in the livers *in vivo,* NR2F1 loss of function invariably led to enhanced growth. This was striking *in vivo* as loss of NR2F1 via KO led to relentless growth in the liver of cells delivered *via* intra-splenic injection or directly to the liver. This data supports the fact that NR2F1 at least in the two UM models we explored serves as a natural and spontaneous barrier to metastatic progression through the induction of a state of dormancy. This finding agrees with our previous studies that showed NR2F1 suppresses growth and metastasis burden in various cancer models [56,71]. High YAP1 activity reported to be critical for survival of UM cells [64 59]. We found that invariably the YAP1 pathway was negatively regulated by NR2F1 and forced downregulation of NR2F1 led to a putative de-repression of YAP1/TEAD1 genes and activated YAP oncogenic signaling. YAP1 expression was also absent in solitary cells in 3D models or in solitary UM DCCs *in vivo* and in humans or in small clusters but became detectable in metastatic cores in humans and large cluster in 3D cultures and in the mouse liver UM metastasis. Perhaps combined detection of YAP1 and NR2F1 levels in metastasis resected as a treatment may more firmly inform on disease progression and therapy responses in those patients.

The gain of function tools to increase NR2F1 mRNA and protein dosage also revealed that NR2F1 can actively downregulate YAP1 and TEAD1 mRNA and protein levels. This showed *via* the detection of YAP1/TEAD1 complexes using co-immunoprecipitation, that loss of these two TFs, through a mass effect, reduced the availability of YAP1/TEAD1 transcriptional complexes required for the Gαq/11 oncogene to execute its growth promoting function. This led us to test whether inhibition of the Gαq/11 oncogene could in fact have a reciprocal effect in NR2F1, enabling UM cells to restore NR2F1 expression. This was confirmed when we treated UM OMM1.3 cells with YM, a small molecule inhibitor of Gαq/11,

which led to a reduction of YAP1 expression in UM cells and a strong upregulation of NR2F1 followed by a strong growth arrest. Thus, as targeted therapies emerge for UM and the Gαq/11 oncogene, it is likely that induction of dormancy might be an expected outcome of such therapies. This may offer an opportunity for maintenance therapies using epigenetic therapies that maintain the NR2F1 program [58] and/or using NR2F1 agonists [56] that maintain its function during or following Gαq/11 inhibitor treatments.

The above findings led us to explore how NR2F1 interferes with Gαq/11 oncogene signaling by limiting the availability of YAP1 and TEAD1 complexes. NR2F1 is a nuclear receptor and has *bona fide* target genes during development and in adult cells but it also can interact with retinoic acid receptors to drive lineage commitment and differentiation programs [72,73]. It has also been shown that NR2F1 can act as a transcriptional repressor [74]. Thus, our hypothesis explored whether NR2F1 *via* its transcriptional function could silence YAP1 expression. It has been recently shown that an entire cluster of transcriptional factors that regulates neural-crest and melanocytic differentiation bound YAP responsive elements [75]. Our ChIP data identified that NR2F1 also binds to a specific region of the YAP1 promoter leading to a loss of histone H3 activation mark and reducing the rate of transcription of YAP1 and thus reducing the availability of this TF for complex formation. NR2F1 did however not change the levels of histone H3 repressive marks, suggesting that additional signals may be required to more stably repress YAP1 expression. These results further prompted us to explore the wider transcriptional and chromatin remodeling program that NR2F1 regulates because as mentioned above these UM cells seems to have enough NR2F1 expression to engage a dormancy program simply upon low density 3D culture or upon colonizing the cells as solitary DCCs or small DCC clusters. RNA-seq and Cut & Run assays to dissect NR2F1 regulation of gene transcription revealed complementary information on the programs controlled by NR2F1 in dormant UM cells.

RNA-seq data confirmed that indeed NR2F1 regulates genes related to regulation of gene transcription, neural crest cell migration, axonogenesis and biosynthetic pathways. Interestingly and supporting an anti-UM metastatic function of NR2F1 we found that genes linked to metastatic outgrowth such as NUP210, WNT5AA, SFRP1 and PPAR-γ were repressed by NR2F1. This might explain the aggressive metastatic outgrowth observed upon NR2F1 downregulation and how NR2F1 may ensure dormancy of UM cells by limiting the response to these cues from autocrine or paracrine sources. Further, NR2F1 inhibits genes related to epithelial cell proliferation (SEMA5A, SFRP1, WNT5A, IGF1, SOX9), cell differentiation (SFRP1, IGFBP3, PPARG, ASB4, SOX9, IGF1) and epithelial to mesenchymal transcription (WNT5A, SOX9, IGF1) pathways. An unexpected, but in retrospective, logical result from our RNA-seq was that NR2F1 repressed a strong activator of GPCR signaling, GNAO1 which interacts with proteins that constitutes network of other G protein signaling genes required for G-protein signaling for proliferation. GNAO1 is shown to be linked with the functional differentiation of neurons in the developing brain and shown to promoter growth pathways in HCC and interacts with Phospholipase C (PLC) upstream of ERK/MEK pathway activated in UM [76,77]. In support of GNAO1 repression by NR2F1, we also found negative regulation of GPCR signaling by NR2F1 as revealed by the CUT & RUN analysis. NR2F1-led accumulation of histone H3 repressive marks showed that this TF repressed GPCR signaling associated with glutamate, muscarinic, GABA receptor pathways. This may represent genes associated with those pathways and or the regulation by the peripheral nervous system as it has been shown for other metastatic cancer lesions. Interestingly some of the GPCR pathway regulated genes were already associated with metastasis promotion in different cancers (e.g., GRM3, GRM8, RXFP1) [78–80]. The pathways associated with the genes linked to active histone modifications in NR2F1^{hi} UM cells revealed also a synaptic signaling pathway but how they may be linked to the induction of a dormant DCC phenotype is unknown.

In more general terms, our findings reveal a concept that may be applicable to other cancers: powerful oncogenic signaling can be overridden by transcriptional programs that short-circuit the

oncogene signaling. Conceptually this supports that in UM and other cancers where we have found a similar principle, chromatin remodeling and transcriptional regulation for example by NR2F1, ZFP281 or DEC2 can be under certain contexts and for a long time dominant over the genetic driver mechanisms. Since DCC dormancy seems to be inextricably linked to microenvironmental regulation the next important question in UM, is to determine which are the microenvironmental signals, niches, and cell types that control UM DCC dormancy mainly in the liver but also in other sites. This is important because it may also reveal what microenvironmental changes may alter pro-dormancy niches and allow for UM DCC awakening. Similarly, it will be interesting to establish if there is a developmental link between NR2F1 transcriptional function and activation in the control of GPCR signaling as this may also open a deeper mechanistic understanding of UM metastatic progression and new therapeutic opportunities.

Acknowledgements

We thank the Aguirre-Ghiso and Aplin labs as well as the Gutkind lab and Dr. Liliana Ossowski for helpful discussions. This work was supported by The National Institute of Health (NIH) /National Cancer Institute (NCI) (CA253977, CA109182, CA216248, CA218024, CA013330), DOD-MRP ME200152, ME200270P2, the Samuel Waxman Cancer Research Foundation Tumor Dormancy Program and The Mark Foundation Aspire program and The Gurwin Foundation to J.A.A.G, who is also a Samuel Waxman Cancer Research Foundation Investigator. M.L.A. was recipient of a of a contract from Generalitat Valenciana (APOSTD2019/053). J.A.A.G and A.P. were also supported by a grant from the Falk Foundation. A.E. Aplin has ownership interest in patent number 9880150 and has a pending patent, PCT/US22/76492. J.T is co-inventor for the patent 9880150. No disclosures were reported by other authors.

Author's contribution

R.K. planned, designed, performed experiments, analyzed data, and wrote the manuscript. M.L.A planned and conducted experiments and analyzed data. T.J.P designed and analyzed RNA-seq data. V.C generated inducible cell lines and performed experiments. L.S contributed to discussion and analysis of IF data. J.T developed reagents and performed experiment. M.A.N wrote and edited the manuscript, provided scientific advice, and secured funding. T.S, M.T, R.S.S & L.D.K provided access to human samples (FFPE slides) used in this study. D.Z analyzed Cut & Run data. J.A.G conceived the project, designed the experiments along with A.E.A. J.A.G supervised the project, secured funding, and wrote the manuscript.

Declaration of Interests

J.A.A-Ghiso is a scientific co-founder, scientific advisory board member at, and equity owner in HiberCell and receives financial compensation as a consultant for HiberCell, a Mount Sinai spin-off company focused on therapeutics that prevent or delay cancer recurrence. A.E. Aplin has ownership interest in patent number 9880150 and has a pending patent, PCT/US22/76492. J.T is co-inventor in patent number 9880150. No disclosures were reported by other authors. No other authors have any disclosures.
Author's declare no conflict of interest.

Conflict of interest

Author's declare no conflict of interest.

Figure legends

Fig. 1. Long-lived dormancy of human UM DCCs in mouse livers: A) Scheme depicting the reporter construct used to generate OMM1.3 quiescence reporter (QR) cell line. **B)** Scheme depicting the *in-vivo* experimental strategy for intra-splenic injection, liver colonization and timeline for isolating QR^+/QR^- cells. **C)** Percentage of dormant and proliferative UM cells disseminated to the liver determined by FACS sorting * $p < 0.05$ Mann-Whitney test; n.s non-significant. **D)** Representative images of the liver surface showing solitary OMM1.3-QR^+ DCCs (Top) or OMM1.3-QR^- proliferative micro-metastasis (Bottom) 3 months after intrasplenic injection. **E)** A volcano plot showing differentially expressed genes (RNA-seq) in dormant OMM1.3-QR^+ and proliferative OMM1.3-QR^-. **F&G)** Biological pathways and processes upregulated and downregulated in dormant OMM1.3-QR^+ DCCs based using the Enrichr KG program. **H)** Heatmap showing top 50 significantly upregulated and downregulated genes in dormant and proliferative OMM1.3-QR cells . Arrows indicate cell cycle regulatory genes downregulated (black) and neural-related genes upregulated (purple) in dormant OMM1.3-QR^+ DCCs.

Fig. 2. Dormant solitary UM DCCs express high NR2F1 and regulate neural and cell cycle programs: A) Graph showing expression of neural crest genes upregulated in OMM1.3-QR^+ UM DCCs as revealed from RNA-seq DEG. **B)** NR2F1 mRNA expression in OMM1.3 QR^+/QR^- FACS sorted cells isolated from the livers of mice after 3 months. **C)** Representative IF images of solitary or <8 cell cluster and >8 cells cluster of UM004 **(left panel)** and OMM1.3 **(right panel)** cells disseminated to the liver and stained for NR2F1 and HMB45. The graphs (lower panel) show the percentage of NR2F1 positive cells in each bin of cell cluster categories. Cells having strong HMB45 staining were used to quantify co-stained NR2F1. **D)** IF images (left) and quantification (right) for the expression of NR2F1 (green) in solitary or > 8 cell clusters of OMM1.3 cells cultured in 3D Matrigel. **E)** IF images showing NR2F1 expression (pink) in solitary DCCs or isolated small clusters (left column) or small UM cell clusters (middle column) at the metastasis-liver edge and in the tumor core (right column) in metastatic UM patient samples. The dotted squares in the panel are shown as a zoom-in view across the right side. Graphs represent quantification of NR2F1 expression level (mean fluorescent intensity, MFI) in the nucleus for the above-stained patients.

Fig. 3. Antagonism between NR2F1 and YAP1 regulates proliferation of UM cells: A) Graph showing expression of YAP1, TEAD's, and YAP1 downstream target genes in OMM1.3 QR^+ cells as analyzed from RNA-seq data. **B)** YAP1 mRNA expression in OMM1.3 QR^+ (dormant) vs. QR^- (proliferative) cells at 3 months. **C**) IF images showing expression of YAP1 (red) in OMM1.3 solitary and >2 cell cluster cultured in 3D Matrigel. The graph shows quantification of nuclear MFI of YAP1 in solitary and >2 cells nuclei. **D)** Representative images of colonies formed by Dox-treated OMM1.3 cells transiently transfected with control or NR2F1-targeting siRNAs at day 7- and 14-days post-seeding, showing H2B-GFP and TdT expression. **E)** H2B-GFP label retention at day 7 and 14 in control and NR2F1 knockdown cells (Mann-Whitney test). **F)** Graph showing single cell and > 8-cluster cell colonies formed by control and NR2F1 knockdown OMM1.3 cells cultured on 3D Matrigel. **G)** Fold change in mRNA expression of indicated genes in OMM1.3 control or NR2F1 knockdown cells. **H)** Graph showing number of colonies (only cells > 8-cells were included in quantification) upon YAP1 KD. **I)** Representative IF images (left) and graphs (right) showing expression of YAP1 (green) and NR2F1 (red) in colonies formed by OMM1.3 control and YAP1 knockdown cells at day 7. **J)** Western blots showing expression of NR2F1, YAP1 and TEAD1 in uninduced (No Dox) and induced (Dox treated) UM004 cells. **K)** Graph showing colonies formed by uninduced and Dox-induced NR2F1 over-expressing UM004 cells after 7 days. **L)** Western blots showing expression of NR2F1 and YAP1 in UM004 control and NR2F1 KD cells. **M)** Graph showing events of colonies for control and NR2F1 KD UM004 cells at day 7 (n= 3). **N)** IF images of UM004 solitary and clusters DCCs showing expression of YAP1 post 3 months of UM004 cells dissemination to liver. Zoom-in images are shown in the same panel with marked boundaries indicating YAP1 protein expression. **O)** IF images showing expression of YAP1 and NR2F1 in solitary or small UM cell clusters in UM patient liver

samples. Graphs show the quantification of the MFI of nuclear YAP1 and NR2F1 (arbitrary units A.U.) in solitary and big clusters (proliferative lesion) in UM patient liver samples.

Fig. 4. NR2F1 inhibits functional complex formation between YAP1-TEAD1 serving as a barrier to metastasis:
A&B) Western blots showing expression of indicated proteins in control and NR2F1 knockout OMM1.3 cells, and UM004 untreated or treated with dox to induce NR2F1 expression. A double asterisk indicates a non-specific band. Densitometric quantification (n=3) of YAP1 and TEAD1 expression levels in the OMM1.3 cell line is also shown. **C&D)** OMM1.3 and UM004 treated cells as in **A** processed for Immunoprecipitation (IP) with anti-TEAD1 antibodies followed by immunoblotting with anti-YAP1 antibodies. 10% of input and IgG antibodies were used as internal control and IgG was used as a negative control. **E)** Representative images of melanospheres (n=3) formed by control and CRISPR/cas9 NR2F1 KO OMM1.3 cells after 14 days in the organoid medium. Lower panel shows the quantification of average size of melanospheres in control and NR2F1 KO OMM1.3 cells. (Mann-Whitney test, p-value < 0.0001). **F)** Representative images of livers isolated 3 months after intra-splenic injection of OMM1.3 control and NR2F1-KO cells. The images presented here represent the extreme case of liver metastatic burden, and not all animals showed such massive growth. **G)** Images showing vimentin expression in mouse livers injected with OMM1.3 cells after 3 months to quantify metastatic burden (upper row). The middle row is the zoom-in view of the marked area, showing the morphology of disseminated UM cells in the liver. The lower row shows IF images of the same sections stained with HMB45 (green) antibody. The right panel shows the quantification of metastatic area calculated using vimentin-positive cells (p-value *<0.05 and **<0.02). **H** IF images showing expression of YAP1 in small UM cell clusters and proliferative lesions in mouse liver injected intra-splenically with OMM1.3 control and NR2F1-KO cells.

Fig. 5. NR2F1 negatively regulates oncogenic YAP1 expression and inhibits expression of GPCR family gene GNAO1: A) Schematic showing primer pairs used for scanning the putative binding site of NR2F1 on YAP1 genomic locus (1000 bp upstream of TSS) **B)** NR2F1 ChIP-qPCR analysis in OMM1.3 cells shows the recruitment of NR2F1 upstream of the TSS of the YAP1 promoter. Isotype-matched IgG was used as negative antibody control. **C&D)** ChIP-qPCR showing enrichment of histone carrying activation marks (H3K4me3 & H3K27ac) and repression (H3K9me3) marks at the YAP1 gene using primer pair (-320bp) in OMM1.3 control and NR2F1 knockout cells, and UM004 dox-inducible NR2F1 cells. NR2F1 occupancy onto YAP1 genomic locus in UM004 cells was analyzed using primer pair (-320bp); n= 3, error bars = SD, p-values * < 0.05, ** < 0.02 and *** < 0.01. **E)** Volcano plot showing DEGs in OMM1.3 control and NR2F1 KO cells. **F)** Heatmap showing significantly upregulated and downregulated genes in OMM1.3 control and NR2F1 KO cells using RNA-seq data based on unbiased clustering and p-adj values. **G&H)** Distribution of biological pathways and processes predicted to be upregulated and downregulated as ranked by log_2FC from the top 100 upregulated and downregulated genes in NR2F1 KO OMM1.3 cells compared to control OMM1.3 cells using the Enrichr program.

Fig. 6 NR2F1-induced chromatin remodeling represses GPCR pathway; inhibition of Gαq signaling upregulates NR2F1: A & B) Cut&Run analysis for H3K27me3 and H3K27ac marks was performed in control and NR2F1 KO OMM1.3 cell lines. Genomic regions with differences in signals were identified, and peaks with significant signal enrichment in either control or NR2F1 KO cells are shown as dot plots (right); CPM (average counts per million reads in a peak). **C&D)** Distribution of biological processes predicted to be modulated in NR2F1 KO cells based on differential peaks called for H3K27me3 mark as analyzed by Enrichr program. **E)** Distribution of H3K27me3 and H3K27ac peaks for YAP1 gene in control and NR2F1 KO condition (only one replicate is shown here). Tracks are normalized and scaled to the range by the integrative genomic viewer (IGV). **F)** Graph showing quantification of colonies formed by

OMM1.3 cells grown on Matrigel after 14 days treated with DMSO and compound YM with different concentrations. **G)** Graph showing quantification of NR2F1 positive cells (< and > 8-cells cluster) following treatment with compound YM at different concentrations. **H)** Representative IF images showing expression of YAP1 (red) in colonies formed by OMM1.3 cells treated with 300nM of YM for 14 days and corresponding quantification of YAP1 positive cells (p-value < 0.05, *students t-test*).

References:

1. Economou, M.A., All-Ericsson, C., Bykov, V., Girnita, L., Bartolazzi, A., Larsson, O., and Seregard, S. (2008). Receptors for the liver synthesized growth factors IGF-1 and HGF/SF in uveal melanoma: intercorrelation and prognostic implications. Acta Ophthalmol. *86*, 20–25. 10.1111/j.1755-3768.2008.01182.x.

2. Singh, A.D., Turell, M.E., and Topham, A.K. (2011). Uveal Melanoma: Trends in Incidence, Treatment, and Survival. Ophthalmology *118*, 1881–1885. 10.1016/j.ophtha.2011.01.040.

3. Kujala, E., Mäkitie, T., and Kivelä, T. (2003). Very long-term prognosis of patients with malignant uveal melanoma. Investig. Ophthalmol. Vis. Sci. *44*, 4651–4659. 10.1167/iovs.03-0538.

4. Diener-West, M., Reynolds, S.M., Agugliaro, D.J., Caldwell, R., Cumming, K., Earle, J.D., Hawkins, B.S., Hayman, J.A., Jaiyesimi, I., Jampol, L.M., et al. (2005). Development of Metastatic Disease After Enrollment in the COMS Trials for Treatment of Choroidal Melanoma: Collaborative Ocular Melanoma Study Group Report No. 26. Arch. Ophthalmol. *123*, 1639–1643. 10.1001/archopht.123.12.1639.

5. Bedikian, A.Y., Legha, S.S., Mavligit, G., Carrasco, C.H., Khorana, S., Plager, C., Papadopoulos, N., and Benjamin, R.S. (1995). Treatment of uveal melanoma metastatic to the liver. A review of the M. D. Anderson cancer center experience and prognostic factors. Cancer *76*, 1665–1670. 10.1002/1097-0142(19951101)76:9<1665::aid-cncr2820760925>3.0.co;2-j.

6. Albert, D.M., Ryan, L.M., and Borden, E.C. (1996). Metastatic Ocular and Cutaneous Melanoma: A Comparison of Patient Characteristics and Prognosis. Arch. Ophthalmol. *114*, 107–108. 10.1001/archopht.1996.01100130103030.

7. Bedikian, A.Y. (2006). Metastatic Uveal Melanoma Therapy: Current Options. Int. Ophthalmol. Clin. *46*, 151–166. 10.1097/01.iio.0000195852.08453.de.

8. Gragoudas, E.S., Egan, K.M., Seddon, J.M., Glynn, R.J., Walsh, S.M., Finn, S.M., Munzenrider, J.E., and Spar, M.D. (1991). Survival of Patents with Metastases from Uveal Melanoma. Ophthalmology *98*, 383–390. 10.1016/s0161-6420(91)32285-1.

9. Kath, R., Hayungs, J., Bornfeld, N., Sauerwein, W., Höffken, K., and Seeber, S. (1993). Prognosis and treatment of disseminated uveal melanoma. Cancer *72*, 2219–2223. 10.1002/1097-0142(19931001)72:7<2219::aid-cncr2820720725>3.0.co;2-j.

10. Hassel, J.C., Piperno-Neumann, S., Rutkowski, P., Baurain, J.-F., Schlaak, M., Butler, M.O., Sullivan, R.J., Dummer, R., Kirkwood, J.M., Orloff, M., et al. (2023). Three-Year Overall Survival with Tebentafusp in Metastatic Uveal Melanoma. N. Engl. J. Med. 10.1056/nejmoa2304753.

11. Bagge, R.O., Nelson, A., Shafazand, A., All-Eriksson, C., Cahlin, C., Elander, N., Helgadottir, H., Kiilgaard, J.F., Kinhult, S., Ljuslinder, I., et al. (2023). Isolated Hepatic Perfusion With Melphalan for Patients With Isolated Uveal Melanoma Liver Metastases: A Multicenter, Randomized, Open-Label, Phase III Trial (the SCANDIUM Trial). J. Clin. Oncol. *41*, 3042–3050. 10.1200/jco.22.01705.

12. Robertson, A.G., Shih, J., Yau, C., Gibb, E.A., Oba, J., Mungall, K.L., Hess, J.M., Uzunangelov, V., Walter, V., Danilova, L., et al. (2018). Integrative Analysis Identifies Four Molecular and Clinical Subsets in Uveal Melanoma. Cancer Cell *33*, 151. 10.1016/j.ccell.2017.12.013.

13. Johansson, P., Aoude, L.G., Wadt, K., Glasson, W.J., Warrier, S.K., Hewitt, A.W., Kiilgaard, J.F., Heegaard, S., Isaacs, T., Franchina, M., et al. (2015). Deep sequencing of uveal melanoma identifies a recurrent mutation in PLCB4. Oncotarget *7*, 4624–4631. 10.18632/oncotarget.6614.

14. Onken, M.D., Worley, L.A., Long, M.D., Duan, S., Council, M.L., Bowcock, A.M., and Harbour, J.W. (2008). Oncogenic mutations in GNAQ occur early in uveal melanoma. Investig. Ophthalmol. Vis. Sci. *49*, 5230–5234. 10.1167/iovs.08-2145.

15. Raamsdonk, C.D.V., Bezrookove, V., Green, G., Bauer, J., Gaugler, L., O'Brien, J.M., Simpson, E.M., Barsh, G.S., and Bastian, B.C. (2009). Frequent somatic mutations of GNAQ in uveal melanoma and blue naevi. Nature *457*, 599–602. 10.1038/nature07586.

16. D., V.R.C., G., G.K., B., C.M., C., G.M., Swapna, V., Thomas, W., C., O.A., Werner, W., Gary, G., Nancy, B., et al. (2010). Mutations in GNA11 in Uveal Melanoma. N. Engl. J. Med. *363*, 2191–2199. 10.1056/nejmoa1000584.

17. Harbour, J.W. (2012). The genetics of uveal melanoma: an emerging framework for targeted therapy. Pigment Cell Melanoma Res. *25*, 171–181. 10.1111/j.1755-148x.2012.00979.x.

18. Martin, M., Maßhöfer, L., Temming, P., Rahmann, S., Metz, C., Bornfeld, N., Nes, J. van de, Klein-Hitpass, L., Hinnebusch, A.G., Horsthemke, B., et al. (2013). Exome sequencing identifies recurrent somatic mutations in EIF1AX and SF3B1 in uveal melanoma with disomy 3. Nat. Genet. *45*, 933–936. 10.1038/ng.2674.

19. Lake, S.L., Coupland, S.E., Taktak, A.F.G., and Damato, B.E. (2010). Whole-Genome Microarray Detects Deletions and Loss of Heterozygosity of Chromosome 3 Occurring Exclusively in Metastasizing Uveal Melanoma. Investig. Opthalmology Vis. Sci. *51*, 4884. 10.1167/iovs.09-5083.

20. Harbour, J.W., Onken, M.D., Roberson, E.D.O., Duan, S., Cao, L., Worley, L.A., Council, M.L., Matatall, K.A., Helms, C., and Bowcock, A.M. (2010). Frequent Mutation of BAP1 in Metastasizing Uveal Melanomas. Science *330*, 1410–1413. 10.1126/science.1194472.

21. Dono, M., Angelini, G., Cecconi, M., Amaro, A., Esposito, A.I., Mirisola, V., Maric, I., Lanza, F., Nasciuti, F., Viaggi, S., et al. (2014). Mutation frequencies of GNAQ, GNA11, BAP1, SF3B1, EIF1AX and TERT in uveal melanoma: detection of an activating mutation in the TERT gene promoter in a single case of uveal melanoma. Br. J. Cancer *110*, 1058–1065. 10.1038/bjc.2013.804.

22. Ewens, K.G., Kanetsky, P.A., Richards-Yutz, J., Purrazzella, J., Shields, C.L., Ganguly, T., and Ganguly, A. (2014). Chromosome 3 status combined with BAP1 and EIF1AX mutation profiles are associated with metastasis in uveal melanoma. Investig. Ophthalmol. Vis. Sci. *55*, 5160–5167. 10.1167/iovs.14-14550.

23. Kalirai, H., Dodson, A., Faqir, S., Damato, B.E., and Coupland, S.E. (2014). Lack of BAP1 protein expression in uveal melanoma is associated with increased metastatic risk and has utility in routine prognostic testing. Br. J. Cancer *111*, 1373–1380. 10.1038/bjc.2014.417.

24. Koopmans, A.E., Verdijk, R.M., Brouwer, R.W.W., Bosch, T.P.P. van den, Berg, M.M.P. van den, Vaarwater, J., Kockx, C.E.M., Paridaens, D., Naus, N.C., Nellist, M., et al. (2014). Clinical significance of immunohistochemistry for detection of BAP1 mutations in uveal melanoma. Mod. Pathol. *27*, 1321–1330. 10.1038/modpathol.2014.43.

25. Jensen, D.E., Proctor, M., Marquis, S.T., Gardner, H.P., Ha, S.I., Chodosh, L.A., Ishov, A.M., Tommerup, N., Vissing, H., Sekido, Y., et al. (1998). BAP1: a novel ubiquitin hydrolase which binds to the BRCA1 RING finger and enhances BRCA1-mediated cell growth suppression. Oncogene *16*, 1097–1112. 10.1038/sj.onc.1201861.

26. Scheuermann, J.C., Alonso, A.G. de A., Oktaba, K., Ly-Hartig, N., McGinty, R.K., Fraterman, S., Wilm, M., Muir, T.W., and Müller, J. (2010). Histone H2A deubiquitinase activity of the Polycomb repressive complex PR-DUB. Nature *465*, 243–247. 10.1038/nature08966.

27. Carbone, M., Yang, H., Pass, H.I., Krausz, T., Testa, J.R., and Gaudino, G. (2013). BAP1 and cancer. Nat. Rev. Cancer *13*, 153–159. 10.1038/nrc3459.

28. Ismail, I.H., Davidson, R., Gagné, J.-P., Xu, Z.Z., Poirier, G.G., and Hendzel, M.J. (2014). Germline Mutations in BAP1 Impair Its Function in DNA Double-Strand Break Repair. Cancer Res. *74*, 4282–4294. 10.1158/0008-5472.can-13-3109.

29. Yu, H., Pak, H., Hammond-Martel, I., Ghram, M., Rodrigue, A., Daou, S., Barbour, H., Corbeil, L., Hébert, J., Drobetsky, E., et al. (2014). Tumor suppressor and deubiquitinase BAP1 promotes DNA double-strand break repair. Proc. Natl. Acad. Sci. *111*, 285–290. 10.1073/pnas.1309085110.

30. Field, M.G., Decatur, C.L., Kurtenbach, S., Gezgin, G., Velden, P.A. van der, Jager, M.J., Kozak, K.N., and Harbour, J.W. (2016). PRAME as an Independent Biomarker for Metastasis in Uveal Melanoma. Clin. Cancer Res. *22*, 1234–1242. 10.1158/1078-0432.ccr-15-2071.

31. Gill, V.T., Norrman, E., Sabazade, S., Karim, A., Lardner, E., and Stålhammar, G. (2023). Multiorgan Involvement of Dormant Uveal Melanoma Micrometastases in Postmortem Tissue From Patients Without Coexisting Macrometastases. Am. J. Clin. Pathol. *160*, 164–174. 10.1093/ajcp/aqad029.

32. Rodrigues, M., Mobuchon, L., Houy, A., Alsafadi, S., Baulande, S., Mariani, O., Marande, B., Rais, K.A., Kooij, M.K.V. der, Kapiteijn, E., et al. (2019). Evolutionary Routes in Metastatic Uveal Melanomas Depend on MBD4 Alterations. Clin. Cancer Res. *25*, 5513–5524. 10.1158/1078-0432.ccr-19-1215.

33. Shain, A.H., Bagger, M.M., Yu, R., Chang, D., Liu, S., Vemula, S., Weier, J.F., Wadt, K., Heegaard, S., Bastian, B.C., et al. (2019). The genetic evolution of metastatic uveal melanoma. Nat. Genet. *51*, 1123–1130. 10.1038/s41588-019-0440-9.

34. McWilliam, R.J. (1961). DELAYED LOCAL METASTASIS IN A CHOROIDAL MELANOMA*. Br. J. Ophthalmol. *45*, 147. 10.1136/bjo.45.2.147.

35. Harper, K.L., Sosa, M.S., Entenberg, D., Hosseini, H., Cheung, J.F., Nobre, R., Avivar-Valderas, A., Nagi, C., Girnius, N., Davis, R.J., et al. (2016). Mechanism of early dissemination and metastasis in Her2+ mammary cancer. Nature *540*, 588–592. 10.1038/nature20609.

36. Hosseini, H., Obradović, M.M.S., Hoffmann, M., Harper, K.L., Sosa, M.S., Werner-Klein, M., Nanduri, L.K., Werno, C., Ehrl, C., Maneck, M., et al. (2016). Early dissemination seeds metastasis in breast cancer. Nature *540*, 552–558. 10.1038/nature20785.

37. Linde, N., Casanova-Acebes, M., Sosa, M.S., Mortha, A., Rahman, A., Farias, E., Harper, K., Tardio, E., Torres, I.R., Jones, J., et al. (2018). Macrophages orchestrate breast cancer early dissemination and metastasis. Nat. Commun. *9*, 21. 10.1038/s41467-017-02481-5.

38. Logan, P.T., Fernandes, B.F., Cesare, S.D., Marshall, J.-C.A., Maloney, S.C., and Burnier, M.N. (2008). Single-cell tumor dormancy model of uveal melanoma. Clin. Exp. Metastasis *25*, 509–516. 10.1007/s10585-008-9158-2.

39. Rawles, M.E. (1947). Origin of Pigment Cells from the Neural Crest in the Mouse Embryo. Physiol. Zoöl. *20*, 248–266. 10.1086/physzool.20.3.30151958.

40. Harris, M.L., and Erickson, C.A. (2007). Lineage specification in neural crest cell pathfinding. Dev. Dyn. *236*, 1–19. 10.1002/dvdy.20919.

41. Bragado, P., Estrada, Y., Parikh, F., Krause, S., Capobianco, C., Farina, H.G., Schewe, D.M., and Aguirre-Ghiso, J.A. (2013). TGF-β2 dictates disseminated tumour cell fate in target organs through TGF-β-RIII and p38α/β signalling. Nat. Cell Biol. *15*, 1351–1361. 10.1038/ncb2861.

42. Sosa, M.S., Parikh, F., Maia, A.G., Estrada, Y., Bosch, A., Bragado, P., Ekpin, E., George, A., Zheng, Y., Lam, H.-M., et al. (2015). NR2F1 controls tumour cell dormancy via SOX9- and RARβ-driven quiescence programmes. Nat. Commun. *6*, 6170. 10.1038/ncomms7170.

43. Nobre, A.R., Dalla, E., Yang, J., Huang, X., Wullkopf, L., Risson, E., Razghandi, P., Anton, M.L., Zheng, W., Seoane, J.A., et al. (2022). ZFP281 drives a mesenchymal-like dormancy program in early

disseminated breast cancer cells that prevents metastatic outgrowth in the lung. Nat. Cancer *3*, 1165–1180. 10.1038/s43018-022-00424-8.

44. Rada-Iglesias, A., Bajpai, R., Prescott, S., Brugmann, S.A., Swigut, T., and Wysocka, J. (2012). Epigenomic Annotation of Enhancers Predicts Transcriptional Regulators of Human Neural Crest. Cell Stem Cell *11*, 633–648. 10.1016/j.stem.2012.07.006.

45. Ypsilanti, A.R., Pattabiraman, K., Catta-Preta, R., Golonzhka, O., Lindtner, S., Tang, K., Jones, I.R., Abnousi, A., Juric, I., Hu, M., et al. (2021). Transcriptional network orchestrating regional patterning of cortical progenitors. Proc. Natl. Acad. Sci. *118*, e2024795118. 10.1073/pnas.2024795118.

46. Sosa, M.S., Bragado, P., and Aguirre-Ghiso, J.A. (2014). Mechanisms of disseminated cancer cell dormancy: an awakening field. Nat. Rev. Cancer *14*, 611–622. 10.1038/nrc3793.

47. Song, C., Piva, M., Sun, L., Hong, A., Moriceau, G., Kong, X., Zhang, H., Lomeli, S., Qian, J., Yu, C.C., et al. (2017). Recurrent tumor cell-intrinsic and -extrinsic alterations during MAPKi-induced melanoma regression and early adaptation. Cancer Discov. *7*, CD-17-0401. 10.1158/2159-8290.cd-17-0401.

48. Zimmerman, L.E., McLean, I.W., and Foster, W.D. (1978). Does enucleation of the eye containing a malignant melanoma prevent or accelerate the dissemination of tumour cells. Br. J. Ophthalmol. *62*, 420. 10.1136/bjo.62.6.420.

49. Grossniklaus, H.E. (2013). Progression of Ocular Melanoma Metastasis to the Liver: The 2012 Zimmerman Lecture. JAMA Ophthalmol. *131*, 462–469. 10.1001/jamaophthalmol.2013.2547.

50. Challen, G.A., and Goodell, M.A. (2008). Promiscuous Expression of H2B-GFP Transgene in Hematopoietic Stem Cells. PLoS ONE *3*, e2357. 10.1371/journal.pone.0002357.

51. Sugase, T., Lam, B.Q., Danielson, M., Terai, M., Aplin, A.E., Gutkind, J.S., and Sato, T. (2020). Development and optimization of orthotopic liver metastasis xenograft mouse models in uveal melanoma. J. Transl. Med. *18*, 208. 10.1186/s12967-020-02377-x.

52. Ranganathan, A.C., Adam, A.P., Zhang, L., and Aguirre-Ghiso, J.A. (2006). Tumor cell dormancy induced by p38SAPK and ER-stress signaling: An adaptive advantage for metastatic cells? Cancer Biol. Ther. *5*, 729–735. 10.4161/cbt.5.7.2968.

53. Sosa, M.S., Avivar-Valderas, A., Bragado, P., Wen, H.-C., and Aguirre-Ghiso, J.A. (2011). ERK1/2 and p38α/β Signaling in Tumor Cell Quiescence: Opportunities to Control Dormant Residual Disease. Clin. Cancer Res. *17*, 5850–5857. 10.1158/1078-0432.ccr-10-2574.

54. Calvo, V., Zheng, W., Adam-Artigues, A., Staschke, K.A., Huang, X., Cheung, J.F., Nobre, A.R., Fujisawa, S., Liu, D., Fumagalli, M., et al. (2023). A PERK-Specific Inhibitor Blocks Metastatic Progression by Limiting Integrated Stress Response–Dependent Survival of Quiescent Cancer Cells. Clin. Cancer Res. *29*, 5155–5172. 10.1158/1078-0432.ccr-23-1427.

55. Sun, D., Singh, D.K., Carcamo, S., Filipescu, D., Khalil, B., Huang, X., Miles, B.A., Westra, W., Sproll, K.C., Hasson, D., et al. (2022). MacroH2A impedes metastatic growth by enforcing a discrete dormancy program in disseminated cancer cells. Sci. Adv. *8*, eabo0876. 10.1126/sciadv.abo0876.

56. Khalil, B.D., Sanchez, R., Rahman, T., Rodriguez-Tirado, C., Moritsch, S., Martinez, A.R., Miles, B., Farias, E., Mezei, M., Nobre, A.R., et al. (2021). An NR2F1-specific agonist suppresses metastasis by inducing cancer cell dormancy. J. Exp. Med. *219*, e20210836. 10.1084/jem.20210836.

57. Borgen, E., Rypdal, M.C., Sosa, M.S., Renolen, A., Schlichting, E., Lønning, P.E., Synnestvedt, M., Aguirre-Ghiso, J.A., and Naume, B. (2018). NR2F1 stratifies dormant disseminated tumor cells in breast cancer patients. Breast Cancer Res. *20*, 120. 10.1186/s13058-018-1049-0.

58. Singh, D.K., Carcamo, S., Farias, E.F., Hasson, D., Zheng, W., Sun, D., Huang, X., Cheung, J., Nobre, A.R., Kale, N., et al. (2023). 5-Azacytidine- and retinoic-acid-induced reprogramming of DCCs into dormancy suppresses metastasis via restored TGF-β-SMAD4 signaling. Cell Rep. *42*, 112560. 10.1016/j.celrep.2023.112560.

59. Feng, X., Degese, M.S., Iglesias-Bartolome, R., Vaque, J.P., Molinolo, A.A., Rodrigues, M., Zaidi, M.R., Ksander, B.R., Merlino, G., Sodhi, A., et al. (2014). Hippo-Independent Activation of YAP by the GNAQ Uveal Melanoma Oncogene through a Trio-Regulated Rho GTPase Signaling Circuitry. Cancer Cell *25*, 831–845. 10.1016/j.ccr.2014.04.016.

60. Amin, R., Shukla, A., Zhu, J.J., Kim, S., Wang, P., Tian, S.Z., Tran, A.D., Paul, D., Cappell, S.D., Burkett, S., et al. (2021). Nuclear pore protein NUP210 depletion suppresses metastasis through heterochromatin-mediated disruption of tumor cell mechanical response. Nat. Commun. *12*, 7216. 10.1038/s41467-021-27451-w.

61. Saini, S., Liu, J., Yamamura, S., Majid, S., Kawakami, K., Hirata, H., and Dahiya, R. (2009). Functional Significance of Secreted Frizzled-Related Protein 1 in Metastatic Renal Cell Carcinomas. Cancer Res. *69*, 6815–6822. 10.1158/0008-5472.can-09-1254.

62. Sas-Korczyńska, B., Markiewicz, A., Romanowska-Dixon, B., and Pluta, E. (2014). Preliminary results of proton radiotherapy for choroidal melanoma – the Kraków experience. Contemp. Oncol. *18*, 359–366. 10.5114/wo.2014.42233.

63. Yu, F.-X., Luo, J., Mo, J.-S., Liu, G., Kim, Y.C., Meng, Z., Zhao, L., Peyman, G., Ouyang, H., Jiang, W., et al. (2014). Mutant Gq/11 Promote Uveal Melanoma Tumorigenesis by Activating YAP. Cancer Cell *25*, 822–830. 10.1016/j.ccr.2014.04.017.

64. Li, H., Li, Q., Dang, K., Ma, S., Cotton, J.L., Yang, S., Zhu, L.J., Deng, A.C., Ip, Y.T., Johnson, R.L., et al. (2019). YAP/TAZ Activation Drives Uveal Melanoma Initiation and Progression. Cell Rep. *29*, 3200-3211.e4. 10.1016/j.celrep.2019.03.021.

65. Cichorek, M., Wachulska, M., Stasiewicz, A., and Tymińska, A. (2013). Skin melanocytes: biology and development. Adv. Dermatol. Allergol.Post□py Dermatol. Alergol. *30*, 30–41. 10.5114/pdia.2013.33376.

66. Dupin, E., Real, C., Glavieux-Pardanaud, C., Vaigot, P., and Douarin, N.M.L. (2003). Reversal of developmental restrictions in neural crest lineages: Transition from Schwann cells to glial-melanocytic precursors in vitro. Proc. Natl. Acad. Sci. *100*, 5229–5233. 10.1073/pnas.0831229100.

67. Wang, T., Wang, Z., Fabritus, L. de, Tao, J., Saied, E.M., Lee, H.-J., Ramazanov, B.R., Jackson, B., Burkhardt, D., Parker, M., et al. (2021). 1-deoxysphingolipids bind to COUP-TF to modulate lymphatic and cardiac cell development. Dev. Cell *56*, 3128-3145.e15. 10.1016/j.devcel.2021.10.018.

68. Lin, F.-J., Qin, J., Tang, K., Tsai, S.Y., and Tsai, M.-J. (2011). Coup d'Etat: An Orphan Takes Control. Endocr. Rev. *32*, 404–421. 10.1210/er.2010-0021.

69. Faedo, A., Tomassy, G.S., Ruan, Y., Teichmann, H., Krauss, S., Pleasure, S.J., Tsai, S.Y., Tsai, M.-J., Studer, M., and Rubenstein, J.L.R. (2008). COUP-TFI Coordinates Cortical Patterning, Neurogenesis, and Laminar Fate and Modulates MAPK/ERK, AKT, and ß-Catenin Signaling. Cereb. Cortex *18*, 2117–2131. 10.1093/cercor/bhm238.

70. Kim, R.S., Avivar-Valderas, A., Estrada, Y., Bragado, P., Sosa, M.S., Aguirre-Ghiso, J.A., and Segall, J.E. (2012). Dormancy Signatures and Metastasis in Estrogen Receptor Positive and Negative Breast Cancer. PLoS ONE *7*, e35569. 10.1371/journal.pone.0035569.

71. Rodriguez-Tirado, C., Kale, N., Carlini, M.J., Shrivastava, N., Rodrigues, A.A., Khalil, B.D., Bravo-Cordero, J.J., Hong, Y., Alexander, M., Ji, J., et al. (2022). NR2F1 Is a Barrier to Dissemination of Early-Stage Breast Cancer Cells. Cancer Res. *82*, 2313–2326. 10.1158/0008-5472.can-21-4145.

72. Wang, L.-H., Tsai, S.Y., Cook, R.G., Beattie, W.G., Tsai, M.-J., and O'Malley, B.W. (1989). COUP transcription factor is a member of the steroid receptor superfamily. Nature *340*, 163–166. 10.1038/340163a0.

73. Bovetti, S., Bonzano, S., Garzotto, D., Giannelli, S.G., Iannielli, A., Armentano, M., Studer, M., and Marchis, S.D. (2013). COUP-TFI controls activity-dependent tyrosine hydroxylase expression in adult dopaminergic olfactory bulb interneurons. Development *140*, 4850–4859. 10.1242/dev.089961.

74. Cooney, A.J., Tsai, S.Y., O'Malley, B.W., and Tsai, M.-J. (1992). Chicken Ovalbumin Upstream Promoter Transcription Factor (COUP-TF) Dimers Bind to Different GGTCA Response Elements, Allowing COUP-TF To Repress Hormonal Induction of the Vitamin D3, Thyroid Hormone, and Retinoic Acid Receptors. Mol. Cell. Biol. *12*, 4153–4163. 10.1128/mcb.12.9.4153-4163.1992.

75. Barbosa, I.A.M., Gopalakrishnan, R., Mercan, S., Mourikis, T.P., Martin, T., Wengert, S., Sheng, C., Ji, F., Lopes, R., Knehr, J., et al. (2023). Cancer lineage-specific regulation of YAP responsive elements revealed through large-scale functional epigenomic screens. Nat. Commun. *14*, 3907. 10.1038/s41467-023-39527-w.

76. Pei, X., Zhang, J., Wu, L., Lü, B., Zhang, X., Yang, D., and Liu, J. (2013). The down-regulation of GNAO1 and its promoting role in hepatocellular carcinoma. Biosci. Rep. *33*, e00069. 10.1042/bsr20130001.

77. Akamine, S., Okuzono, S., Yamamoto, H., Setoyama, D., Sagata, N., Ohgidani, M., Kato, T.A., Ishitani, T., Kato, H., Masuda, K., et al. (2020). GNAO1 organizes the cytoskeletal remodeling and firing of developing neurons. FASEB J. *34*, 16601–16621. 10.1096/fj.202001113r.

78. Zhang, P., Kang, B., Xie, G., Li, S., Gu, Y., Shen, Y., Zhao, X., Ma, Y., Li, F., Si, J., et al. (2019). Genomic sequencing and editing revealed the GRM8 signaling pathway as potential therapeutic targets of squamous cell lung cancer. Cancer Lett. *442*, 53–67. 10.1016/j.canlet.2018.10.035.

79. Prickett, T.D., Wei, X., Cardenas-Navia, I., Teer, J.K., Lin, J.C., Walia, V., Gartner, J., Jiang, J., Cherukuri, P.F., Molinolo, A., et al. (2011). Exon capture analysis of G protein-coupled receptors identifies activating mutations in GRM3 in melanoma. Nat. Genet. *43*, 1119–1126. 10.1038/ng.950.

80. Klonisch, T., Bialek, J., Radestock, Y., Hoang-Vu, C., and Hombach-Klonisch, S. (2007). Relaxin and Related Peptides. Adv. Exp. Med. Biol. *612*, 104–118. 10.1007/978-0-387-74672-2_8.

81. Dobin, A., Davis, C.A., Schlesinger, F., Drenkow, J., Zaleski, C., Jha, S., Batut, P., Chaisson, M., and Gingeras, T.R. (2013). STAR: ultrafast universal RNA-seq aligner. Bioinformatics *29*, 15–21. 10.1093/bioinformatics/bts635.

82. Frankish, A., Diekhans, M., Ferreira, A.-M., Johnson, R., Jungreis, I., Loveland, J., Mudge, J.M., Sisu, C., Wright, J., Armstrong, J., et al. (2018). GENCODE reference annotation for the human and mouse genomes. Nucleic Acids Res. *47*, gky955-. 10.1093/nar/gky955.

83. Kluin, R.J.C., Kemper, K., Kuilman, T., Ruiter, J.R. de, Iyer, V., Forment, J.V., Cornelissen-Steijger, P., Rink, I. de, Brugge, P. ter, Song, J.-Y., et al. (2018). XenofilteR: computational deconvolution of mouse and human reads in tumor xenograft sequence data. BMC Bioinform. *19*, 366. 10.1186/s12859-018-2353-5.

84. Li, B., and Dewey, C.N. (2011). RSEM: accurate transcript quantification from RNA-Seq data with or without a reference genome. BMC Bioinform. *12*, 323. 10.1186/1471-2105-12-323.

85. Love, M.I., Huber, W., and Anders, S. (2014). Moderated estimation of fold change and dispersion for RNA-seq data with DESeq2. Genome Biol. *15*, 550. 10.1186/s13059-014-0550-8.

86. Kuleshov, M.V., Jones, M.R., Rouillard, A.D., Fernandez, N.F., Duan, Q., Wang, Z., Koplev, S., Jenkins, S.L., Jagodnik, K.M., Lachmann, A., et al. (2016). Enrichr: a comprehensive gene set enrichment analysis web server 2016 update. Nucleic Acids Res. *44*, W90–W97. 10.1093/nar/gkw377.

Materials and methods

1. Cell culture, transfection, and drug treatment

The human OMM1.3 and UM004 (genetically engineered to knockout or overexpress NR2F1 upon Doxycycline treatment) cell lines were maintained in DMEM-F12 supplemented with 1X L-Glutamine, 10% heat-inactivated fetal bovine serum (FBS) and 100U penicillin/0.1 mg/mL streptomycin. All cells were grown at 5% CO_2 and 37°C and regularly tested for mycoplasma. Transient transfection was

performed using Lipofectamine 3000 (Invitrogen) following manufacturer's instructions. siRNA transfection was performed using Lipofectamine RNAi MAX (Invitrogen) following manufacturer's instructions. NR2F1-knockout cell lines were generated using CRISPR-Cas9–targeted genome editing. Briefly, two separate NR2F1 gRNAs (guide 2, 5′-GATCCGCAGGACGACGTGGC-3′; and guide 4, 5′-GGC TGCCGTAGCGCGACGTG-3′) were cloned into pLentiCRISPRv2 (Addgene-52961). An NT gRNA (5′-GTA TTACTGATATTGGTGGG-3′) was used as a control. Lentiviral vectors were produced in HEK293T cells and viral supernatants were used to infect OMM1.3 QR+ cells. Cells were then selected using 2 µg/ml puromycin (Sigma-Aldrich; P8833). NR2F1 knockout was confirmed by Western blot. For NR2F1-inducible UM004 cell line, NR2F1 WT cDNA was cloned into pENTR/D-TOPO and then pLentiHygro3/TO/V-5-DEST. We transfected HEK293 cells were transfected with plasmid and generated lentivirus were used to infect UM004 cells. Expression of NR2F1 was induced using 0.1µg and 1µg of doxycycline for 48 h.

2. Quantitative real-time PCR

RNA was isolated using RNeasy Plus Mini Kit (Qiagen), and cDNA was prepared using Superscript First Strand Synthesis System for RT-PCR Kit (Biorad) following manufacturers' instructions. Quantitative real-time PCR was performed using manufacturers' instructions for SSO advanced SYBR green kit (Biorad) on ABI-qPCR system using equal amount of template (50–100 ng cDNA) per reaction. Obtained values were normalized to housekeeping gene (Tubulin/RPL30/GAPDH) and are presented as fold differences over control or relative mRNA expression using the ΔΔCt method for relative quantifications. Each comparison was made using triplicate reactions and in at least 3 independent experiments. Primer sequences for different analyzed genes are described in detail in (SI Table 4A).

3. Cell sorting

Livers sections were minced and digested with collagenase supplemented with DNase1 enzyme at 37^0 C for 30 minutes followed by RBC lysis and Percoll gradient was carried out isolated UM cells. Collected cells were resuspended in FACS sorting buffer and sent at Albert Einstein FACS core facility for cell sorting using appropriate controls.

4. Western blot analysis

Cells were lysed in ice cold RIPA buffer (Thermofisher) supplemented with protease inhibitor cocktail (PIC from Invitrogen). Each sample protein concentration was calculated using Pierce BCA protein assay kit and a standard BSA curve. 30 µg of total protein from each cell lysate was used for equal loading and were boiled in 4X Laemmli sample buffer for 5 minutes at 95°C. Samples were run on biorad precasted gel in 1X running buffer (Biorad) and transferred to PVDF membranes in 1X transfer buffer (Biorad) according to manufacturer's protocol. Membranes were blocked in 5% milk or BSA in TBST (Tris-buffered saline supplemented with 0.1% Tween-20) buffer. Membranes were incubated with respected primary antibodies as indicated in each figure at 4°C for overnight shaking. Membranes were washed in TBST buffer and incubated with HRP-conjugated secondary antibodies at room temperature for 1 hour. Western blots were developed using pierce supersignal ECL kit on ABI alpha imager. The antibodies used are listed supplementary table S4B.

5. TF Co-immunoprecipitation assay

Sub-confluent cultures of cells were harvested and lysed in ice cold IP lysis buffer (Thermofisher) supplemented with PIC. Protein concentration was estimated using BCA kit as described above and total protein (1–2 mg) from each sample was immunoprecipitated with (TEAD1/YAP1, IgG) antibody using amounts as suggested in the manufacturer's datasheets. Briefly, immunoprecipitated proteins were collected using 40 µl of protein A/G agarose beads and each immune precipitate was washed thrice with

ice cold IP lysis buffer supplemented with PIC and finally eluted in 50 µl of 2X loading dye. Equal amount of protein samples was fractionated on biorad premade ready to use PAGE gels. Immunodetection was done with anti-YAP1, TEAD1, LATS1, NR2F1 and GAPDH antibodies at a dilution of 1:1000 (listed in SI Table 4). For each immunoprecipitation 10% of input lysate and normal mouse IgG were used as internal controls.

6. Three-dimensional (3D) cell morphology studies

3D cell culture assays were performed in either 08-well chambers (Falcon) or in 06 well plates by coating with 80ul or 400 µl/well of Matrigel™ Matrix Growth Factor Reduced (R&D, Cultrex) respectively. Cells were suspended in complete medium supplemented with 2% Matrigel™, plated at a density of 1000/well for 08 well chamber and 0.1×10^6 for both OMM1.3 and UM004 cells respectively and incubated at 37°C for 5–14 days. A fresh layer of complete medium supplemented with Matrigel™ was added following 2 days of incubation, and the medium was replaced every 48 h with fresh DMEM-F12 medium supplemented with 2% Matrigel. Colonies formed after were monitored daily, and images were captured under phase contrast microscope at either 5, 7 or 14 days using inverted phase contrast microscope (Nikon TS100). For label retention, colonies were counted (epifluorescence microscope) for GFP and Td-tomato signal and in more than 04 wells and ratio of GFP^+/Td-tomato positive colonies were calculated. For colony counting and colony proliferation in 3D, cells were seeded in 08 or 06 well as described above and single cell, > 8-cell or <8- cell colonies were counted under the microscopes and photographs were taken at day 05, 07 or 14th day as described for each experiment. For quantification, for each condition (N=4) wells were counted, and data is plotted using graph pad Prism software.

7. Melanosphere assay:

OMM1. control and NR2F1 KO cells were seeded in triplicate on 06- well low attachment plates (3000 cells/well) in mammospehre medium DMEM-F12 containing B27 supplement, EGF and Methylcellulose. Melanosphere formed in each condition were counted on day 14 and photographs were taken from each representative group. For quantification, for each condition (N=4) wells were counted, and data is plotted using graph pad Prism software.

8. Immunofluorescence

OMM1.3 and UM004 cells were cultured in 8-well chambers (Falcon) and fixed with 4% paraformaldehyde/PBS for 20 minutes at room temperature. For 3D cultures cells were seeded (1000 cells/well) in quadruplicate onto Matrigel (R&D, cultrex) in 8-well culture slides as described by Khalil et al (55). Confocal microscopy was performed using Leica SPE confocal microscope. Cells were stained with respected antibodies as listed in the figures and the dilutions and antibodies used are listed in the supplementary table (Supplementary table S4B).

For immunofluorescence on paraffin-embedded tissue sections (FFPE), slides were incubated in xylene (10 minutes twice) followed by graded ethanol rehydration (3 minutes each), and finally washed with water for 5 min twice. Antigen retrieval for was performed in 10 mM antigen retrieval buffer (pH 6) for 45 minutes using a steamer. Tissues were permeabilized in 0.3% TritonX-100 + PBS for 10 minutes. Cultured cells were fixed in 4% formaldehyde on ice for 10 minutes. Tissue sections and cultured cells were blocked with 3% bovine serum albumin (BSA, Fisher Bioreagents) and 5% normal goat serum in PBS for 1 hour at room temperature. Primary antibodies (listed in key table S4B) in blocking buffer were incubated overnight at 4°C followed by washing with PBS supplemented with 0.1% of TritonX- 100 three times and incubation with Alexa Fluor conjugated secondary antibodies (abcam 1:200 dilution) at room temperature for 1-2 hour in the dark. Tissues were washed with PBS three times. Slides were mounted with ProLong Gold Antifade reagent with DAPI. Images were obtained using Leica Software on a Leica SPE confocal microscope and analyzed using ImageJ software.

9. RNA Sequencing

Cells from OMM1.3 control and NR2F1Ko2 cells cultured on 3D Matrigel for 07 days were extracted from Matrigel using cell dissociation buffer with continuous rocking at 4^0 for 2 h. Cells were collected in ice cold 1X PBS and centrifuged and cell pellet was resuspended in RLT lysis buffer provided with Qiagen and RNA was isolated using RNeasy plus micro kit following manufacturer's instructions. RNA samples QC, library preparation and RNA sequencing were performed at institutional genomics core facility. Concentration of RNA samples were estimated by Qubit 2.0 Fluorometer (Life Technologies) and RNA Quality Number (RQN) was checked by Agilent TapeStation 4200 (Agilent Technologies). Poly-A enriched RNA was used to prepare RNA-seq libraries using the NEBNext Ultra RNA Library Prep Kit from Illumina following the manufacturer's protocol (New England Biolabs). The samples were sequenced in a 2 x 75 bp paired-end configuration using the Illumina Nextseq 500 platform. Raw sequence data generated from Illumina NextSeq 500 were converted to FASTQ files and Quality control analysis was performed on fastq files using FastQC (https://www.bioinformatics.babraham.ac.uk/projects/fastqc/). Reads were aligned to the GRCh38 reference genomes using Star aligner [81] and GENCODE [82] gene and transcript annotations. For the *in vivo* dataset, reads were also aligned to GRCm38, and XenofilteR [83] was used to remove any reads of mouse origin. RSEM [84] was used to quantify gene and transcript expression levels. Principal component analysis (PCA) and gene differential expression analysis was performed using DESeq2 [85]. A paired-sample model was used for the *in vivo* dataset to eliminate any mouse-specific effects. PCA plots were rendered via the ggplot2 package (https://ggplot2.tidyverse.org). Heatmaps of normalized gene expression data were generated using the pheatmap package (https://cran.r-project.org/package=pheatmap). Data were analyzed in R (https://www.R-project.org/). Enrichr was used to determine significantly altered pathways [86][83][84].

10. Cut & Run data analysis and data visualization.

OMM1.3 control and NR2F1KO cells cultured in 3D were isolated as explained in section 3. For each reaction 30000 cells were used and pooled as described in the Epicypher manual. The amount of Metstat panel was adjusted according to the number of cells used. Immunoprecipitated DNA was eluted in elution buffer and quantified on Qubit and used for library preparation and sequenced on Illumina NextSeq 500 platform. As recommended, (2 x 50 cycles) paired end sequencing was performed. Raw data generated from Cut&Run paired-end sequencing reads were trimmed with trim galore (v0.6.7; https://github.com/FelixKrueger/TrimGalore) and then mapped to the mouse genome (mm10) using the Bowtie2 (v2.4.5; option -X 2000 –no-mixed –no-discordant). Read pairs with a mapping score >20 was kept for further analysis and duplicated reads due to PCR amplification were removed by SAM tools (v1.9). MACS2 (v 2.2.7.1) were used to call H3K4me3 and H3K27ac peaks in the paired-end mode and default options but for H3K27me3 enriched regions a sliding window method was used. Peaks from control and knockout samples were merged to generate a list of union peaks. Reads from individual samples located at the merged peaks were computed and used for sample clustering and differential modification analysis using the package EdgeR. To compare all three types of H3 modifications together, we counted the numbers of reads in each sample located to the +/- 2000 bp of transcription start sites of all the RefSeq genes and used them to perform principal component analysis. The software deep Tools (v3.5.1) was used for generating heatmaps of read densities centered on peaks, with data normalized to sequencing depths of 10 million. Read coverage was computed with the IGV tools and used for track visualization at IGV.

11. RNA interference assays

OMM1.3 and UMOO4 cells were transfected with gene-specific siRNAs (listed in key resource table) twice at the interval of 24 h at a final concentration of 50 nM, in triplicates in 6-well plates using

Lipofectamine RNAiMax reagent (Invitrogen) according to manufacturer's instructions (Invitrogen). Briefly, cells were treated in 2D with control and NR2F1 or YAP1 siRNA for 48 h using and for 05 days in 3D (new siRNA is replenished every 24h) and later harvested to confirming knockdown at protein and transcript level with NR2F1 and YAP1 specific primers and expression at the protein using specific antibodies for NR2F1 and YAP1 and for downstream biological assays as described for results sections and legends.

12. Chromatin immunoprecipitation (ChIP)

OMM1.3 and UM004 control and NR2F1 KO and NR2F1 overexpressed cells were cross-linked, washed, and lysed according to manufacturer's protocol (EZ-ChIP; Millipore 17–371) with minor modifications. Briefly 1 x 10^6 million of either OMM1.3 or UM004 crosslinked cells for each IP were sonicated using Qsonica bioruptor with power setting of 50 and 30 cycles of 30 s on/off. For each IP, 25ug of chromatin was used for pulling down using antibodies specific to NR2F1, H3K4me, H3K27ac, H3K9me3 and corresponding isotype control. Extracted DNA was extracted from each immunoprecipitated sample from control and test groups (the input sample and ChIP DNA samples) were used for qPCR amplification using primers specific to promoter fragments of the YAP1 and control primers. Control primers (EZ-ChIP 22–004; Millipore) for the human GAPDH and RPL30 were used as an internal and positive control. YAP1 promoter region was identified with data from the University of California, Santa Cruz, Genome Bioinformatics (website, http://genome.ucsc.edu); four different primer pairs were designed for the promoter region of the YAP1 gene using the NCBI primer blast or Primer 3 program (SimGene.com). Primer sequences that were used to amplify YAP1 gene promoter (with position numbers relative to the transcription start site) are shown in schematic of (Fig. 5A) and sequences used are listed in (SI Table 4A).

13. *In vivo* studies

BALB/nu female mice (7 weeks old) were purchased from the Charles River Laboratories and maintained under specific pathogen-free (SPF) conditions. All experiments were carried out according to IACUC guidelines. 2×10^6 of OMM1.3 and UM004 control and NR2F1 knockout or overexpressed cells were resuspended in 30ul of PBS and using aseptic condition, the spleen is accessed through a skin incision made by using a surgical blade, followed by access into the abdominal musculature by using surgical scissors near right lateral recumbency under gas anesthesia. Once the spleen is exposed, using a 27-gauge insulin syringe, cells were carefully injected into the spleen of mice respectively. Animals were monitored as per the IACUC guidelines and groups of mice were euthanized at predetermined times. For each group (N=5) mice were used for each group. For tumor burden experiment, OMM1.3 cells were injected directly into the liver and animals were euthanized after 03 months, the livers were excised and used for FFPE section preparation and for sorting of cells using FACS.

14. Human samples:

Slides from Paraffin-embedded sections from clinically diagnosed UM patients with liver metastasis were obtained from Institute of Curie, Paris and Thomas Jefferson university, Philadelphia as per MTA guidelines. Samples were deidentified and obtained with institutional review board approval. FFPE samples were stained for HMB45 (green), NR2F1/YAP1 (in red). Nuclei were counterstained with DAPI. Several fields of view were assessed under each condition and to track UM solitary cells, UM cells near tumor edge and tumor core. Mean fluorescent intensity (MFI) for both NR2F1 and YAP1 was quantitatively measured using QuPath and HMB45 signal was used to track UM cells.

15. Statistical analysis

To ensure reproducibility, in-vitro experiments were repeated at least three times unless otherwise indicated. Data were expressed as means ± SDs from at least three independent experiments. An unpaired *t*-test was used when the results from two groups were compared. Where shown, P-values were calculated using the unpaired Student's *t*-test, multiple *t-test*, Mann–Whitney, or one-way ANOVA analysis as indicated. A p-value of < 0.05 was considered significant. Graph Pad Prism software was used to generate the graphs and QuPath software was used for analyzing IF images from xenografts and human samples.

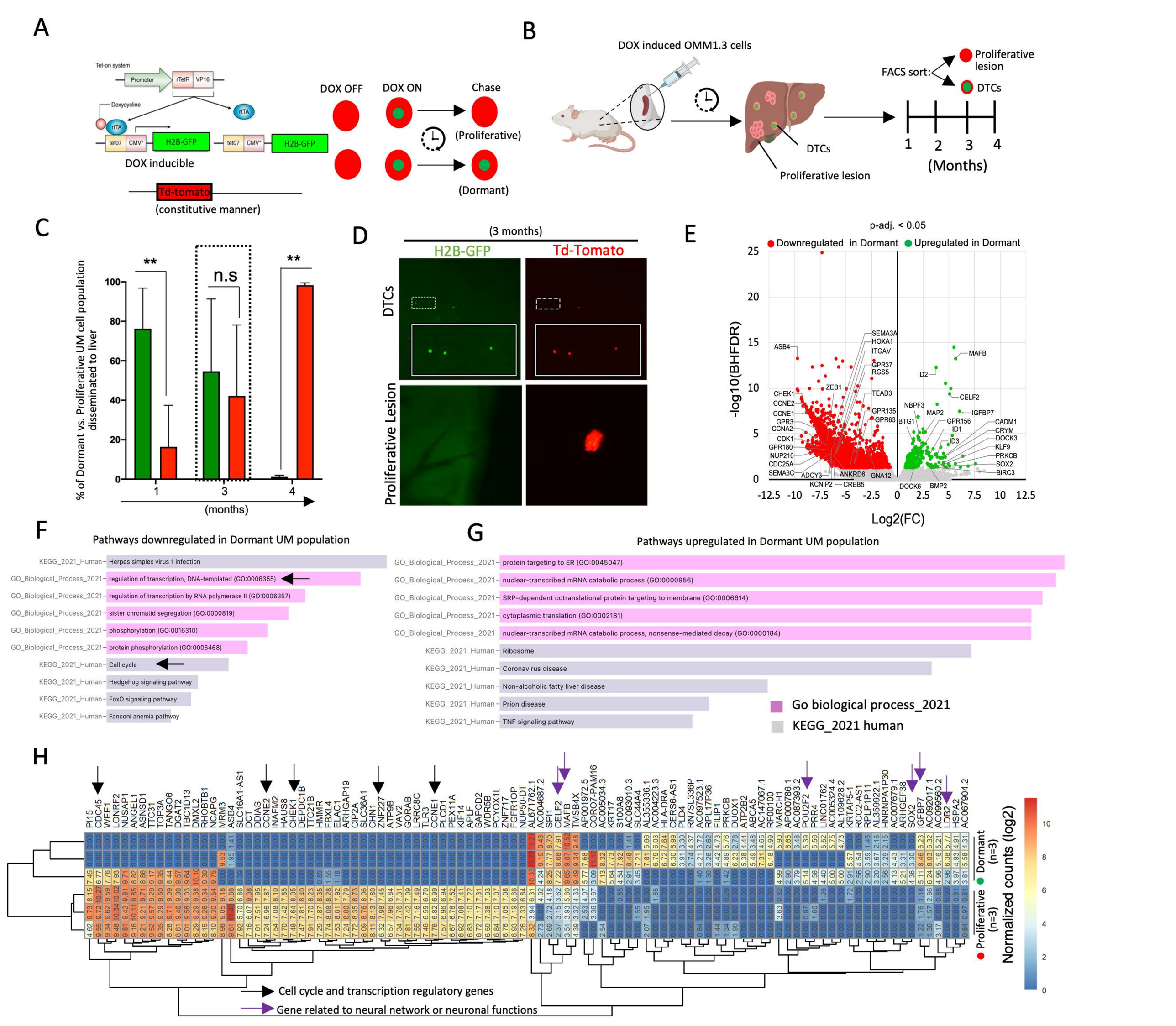
A
Tet-on system
Promoter
rTetR
VP16
Doxycycline
rtTA
tet07
CMV*
H2B-GFP
DOX inducible
Td-tomato
(constitutive manner)
DOX OFF
DOX ON
Chase
(Proliferative)
(Dormant)
B
DOX induced OMM1.3 cells
FACS sort:
Proliferative lesion
DTCs
1
2
3
4
(Months)
C
% of Dormant vs. Proliferative UM cell population disseminated to liver
**
n.s
(months)
D
(3 months)
H2B-GFP
Td-Tomato
DTCs
Proliferative Lesion
E
p-adj. < 0.05
Downregulated in Dormant
Upregulated in Dormant
-log10(BHFDR)
Log2(FC)
F
Pathways downregulated in Dormant UM population
KEGG_2021_Human
Herpes simplex virus 1 infection
GO_Biological_Process_2021
regulation of transcription, DNA-templated (GO:0006355)
regulation of transcription by RNA polymerase II (GO:0006357)
sister chromatid segregation (GO:0000819)
phosphorylation (GO:0016310)
protein phosphorylation (GO:0006468)
Cell cycle
Hedgehog signaling pathway
FoxO signaling pathway
Fanconi anemia pathway
G
Pathways upregulated in Dormant UM population
protein targeting to ER (GO:0045047)
nuclear-transcribed mRNA catabolic process (GO:0000956)
SRP-dependent cotranslational protein targeting to membrane (GO:0006614)
cytoplasmic translation (GO:0002181)
nuclear-transcribed mRNA catabolic process, nonsense-mediated decay (GO:0000184)
Ribosome
Coronavirus disease
Non-alcoholic fatty liver disease
Prion disease
TNF signaling pathway
Go biological process_2021
KEGG_2021 human
H
Cell cycle and transcription regulatory genes
Gene related to neural network or neuronal functions
Proliferative (n=3)
Dormant (n=3)
Normalized counts (log2)

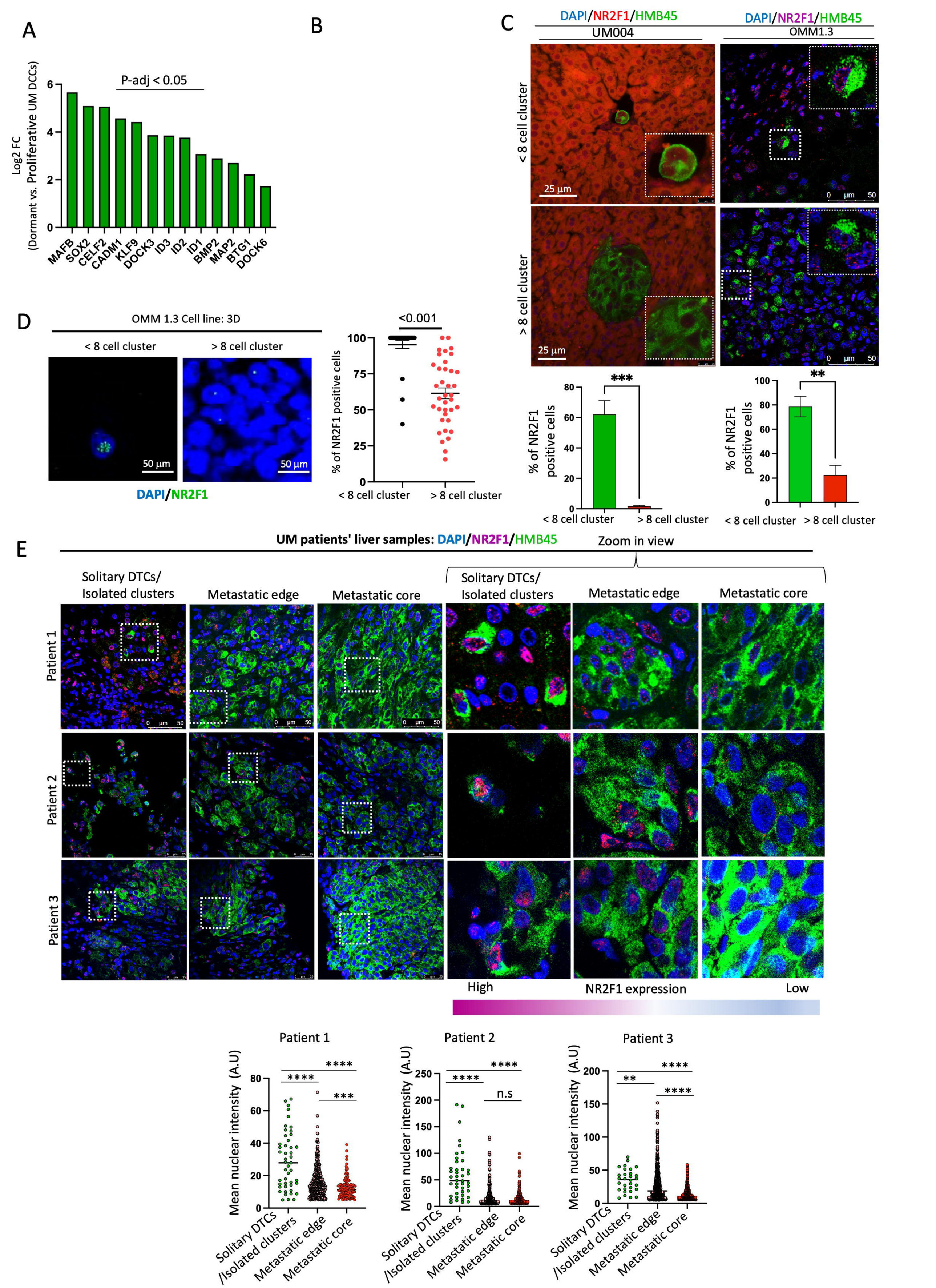
A
P-adj < 0.05
Log2 FC
(Dormant vs. Proliferative UM DCCs)
MAFB
SOX2
CELF2
CADM1
KLF9
DOCK3
ID3
ID2
ID1
BMP2
MAP2
BTG1
DOCK6
B
C
DAPI/NR2F1/HMB45
UM004
OMM1.3
< 8 cell cluster
> 8 cell cluster
25 µm
0 µm 50
% of NR2F1 positive cells
***
**
D
OMM 1.3 Cell line: 3D
< 8 cell cluster
> 8 cell cluster
50 µm
DAPI/NR2F1
<0.001
% of NR2F1 positive cells
E
UM patients' liver samples: DAPI/NR2F1/HMB45
Zoom in view
Solitary DTCs/
Isolated clusters
Metastatic edge
Metastatic core
Patient 1
Patient 2
Patient 3
High
NR2F1 expression
Low
Mean nuclear intensity (A.U)
****
***
**
n.s

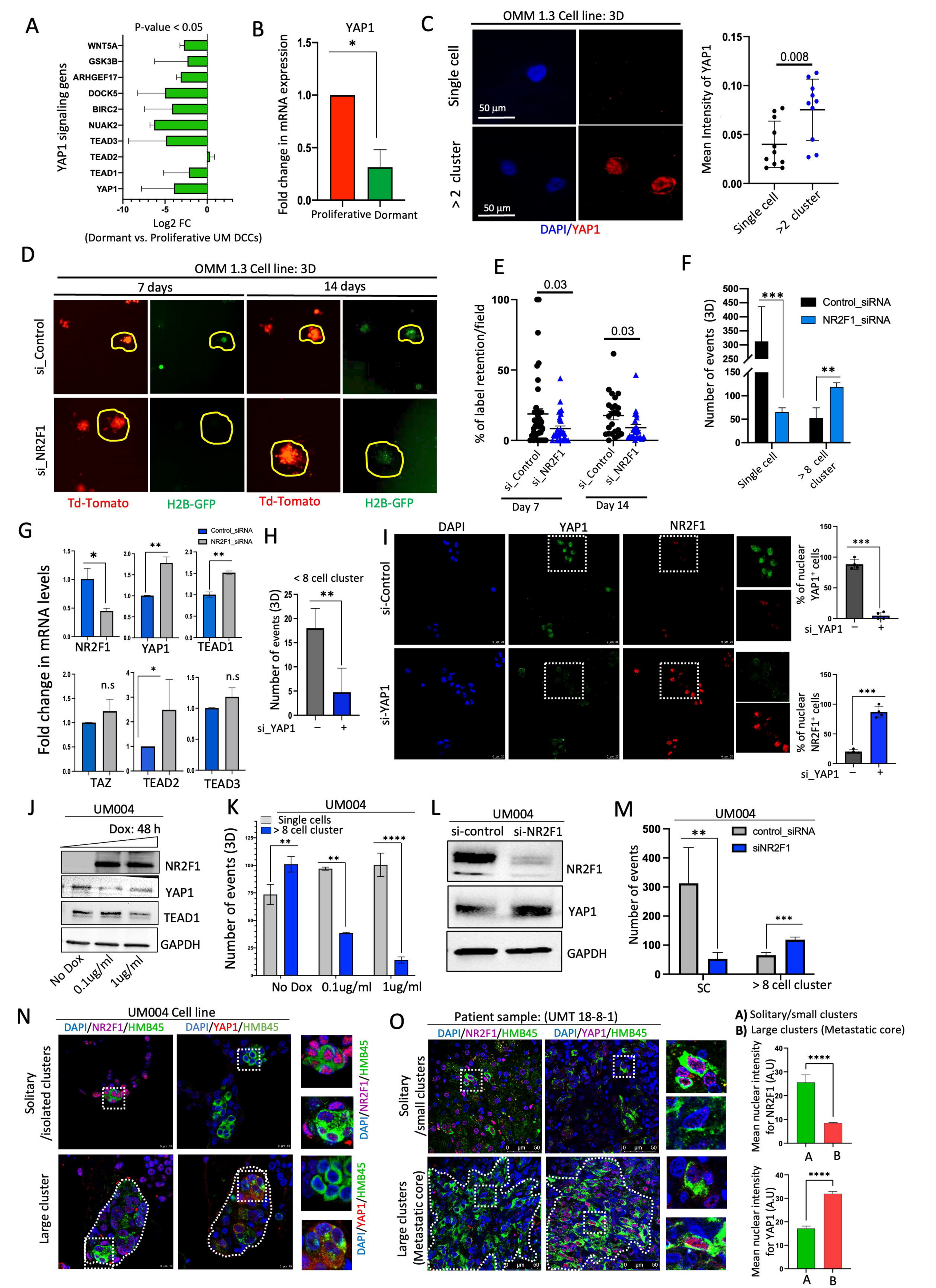
A
P-value < 0.05
YAP1 signaling gens
WNT5A
GSK3B
ARHGEF17
DOCK5
BIRC2
NUAK2
TEAD3
TEAD2
TEAD1
YAP1
Log2 FC
(Dormant vs. Proliferative UM DCCs)
B
YAP1
Fold change in mRNA expression
Proliferative
Dormant
C
OMM 1.3 Cell line: 3D
Single cell
> 2 cluster
50 µm
DAPI/YAP1
Mean Intensity of YAP1
0.008
Single cell
>2 cluster
D
OMM 1.3 Cell line: 3D
7 days
14 days
si_Control
si_NR2F1
Td-Tomato
H2B-GFP
E
% of label retention/field
0.03
si_Control
si_NR2F1
Day 7
Day 14
F
Number of events (3D)
Control_siRNA
NR2F1_siRNA
Single cell
> 8 cell cluster
G
Control_siRNA
NR2F1_siRNA
Fold change in mRNA levels
NR2F1
YAP1
TEAD1
TAZ
TEAD2
TEAD3
n.s
H
< 8 cell cluster
Number of events (3D)
si_YAP1
I
DAPI
YAP1
NR2F1
si-Control
si-YAP1
% of nuclear YAP1+ cells
% of nuclear NR2F1+ cells
si_YAP1
J
UM004
Dox: 48 h
NR2F1
YAP1
TEAD1
GAPDH
No Dox
0.1ug/ml
1ug/ml
K
UM004
Single cells
> 8 cell cluster
Number of events (3D)
No Dox
0.1ug/ml
1ug/ml
L
UM004
si-control
si-NR2F1
NR2F1
YAP1
GAPDH
M
UM004
control_siRNA
siNR2F1
Number of events
SC
> 8 cell cluster
N
UM004 Cell line
DAPI/NR2F1/HMB45
DAPI/YAP1/HMB45
Solitary /isolated clusters
Large cluster
DAPI/NR2F1/HMB45
DAPI/YAP1/HMB45
O
Patient sample: (UMT 18-8-1)
DAPI/NR2F1/HMB45
DAPI/YAP1/HMB45
Solitary /small clusters
Large clusters (Metastatic core)
A) Solitary/small clusters
B) Large clusters (Metastatic core)
Mean nuclear intensity for NR2F1 (A.U)
Mean nuclear intensity for YAP1 (A.U)
A
B

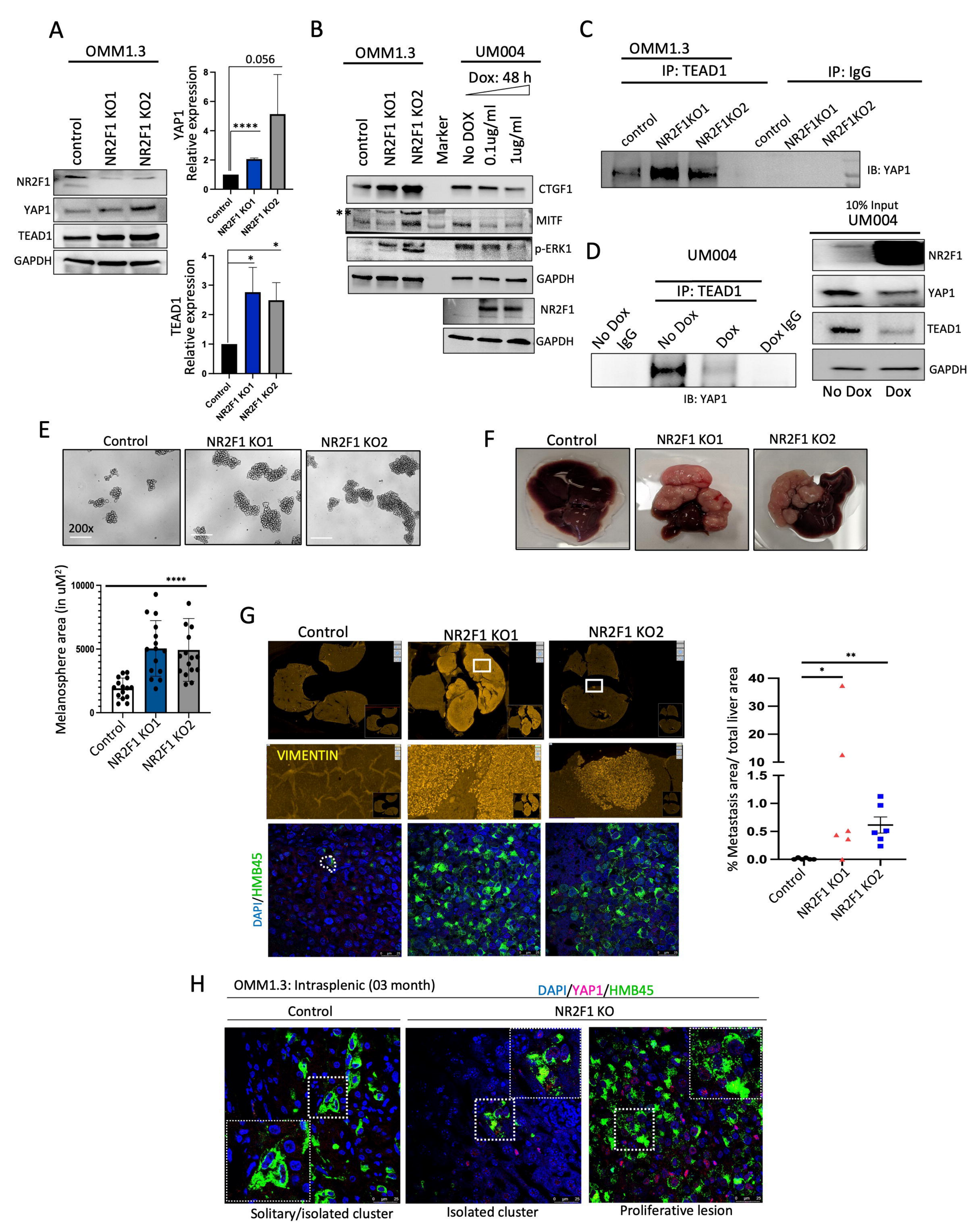
A
OMM1.3
control
NR2F1 KO1
NR2F1 KO2
NR2F1
YAP1
TEAD1
GAPDH
YAP1 Relative expression
0.056
****
Control
NR2F1 KO1
NR2F1 KO2
TEAD1 Relative expression
*
*
B
OMM1.3
UM004
Dox: 48 h
control
NR2F1 KO1
NR2F1 KO2
Marker
No DOX
0.1ug/ml
1ug/ml
CTGF1
MITF
p-ERK1
GAPDH
NR2F1
GAPDH
C
OMM1.3
IP: TEAD1
IP: IgG
control
NR2F1KO1
NR2F1KO2
control
NR2F1KO1
NR2F1KO2
IB: YAP1
D
UM004
IP: TEAD1
No Dox IgG
No Dox
Dox
Dox IgG
IB: YAP1
10% Input
UM004
NR2F1
YAP1
TEAD1
GAPDH
No Dox
Dox
E
Control
NR2F1 KO1
NR2F1 KO2
200x
Melanosphere area (in uM²)
****
Control
NR2F1 KO1
NR2F1 KO2
F
Control
NR2F1 KO1
NR2F1 KO2
G
Control
NR2F1 KO1
NR2F1 KO2
VIMENTIN
DAPI/HMB45
% Metastasis area/ total liver area
**
*
Control
NR2F1 KO1
NR2F1 KO2
H
OMM1.3: Intrasplenic (03 month)
DAPI/YAP1/HMB45
Control
NR2F1 KO
Solitary/isolated cluster
Isolated cluster
Proliferative lesion

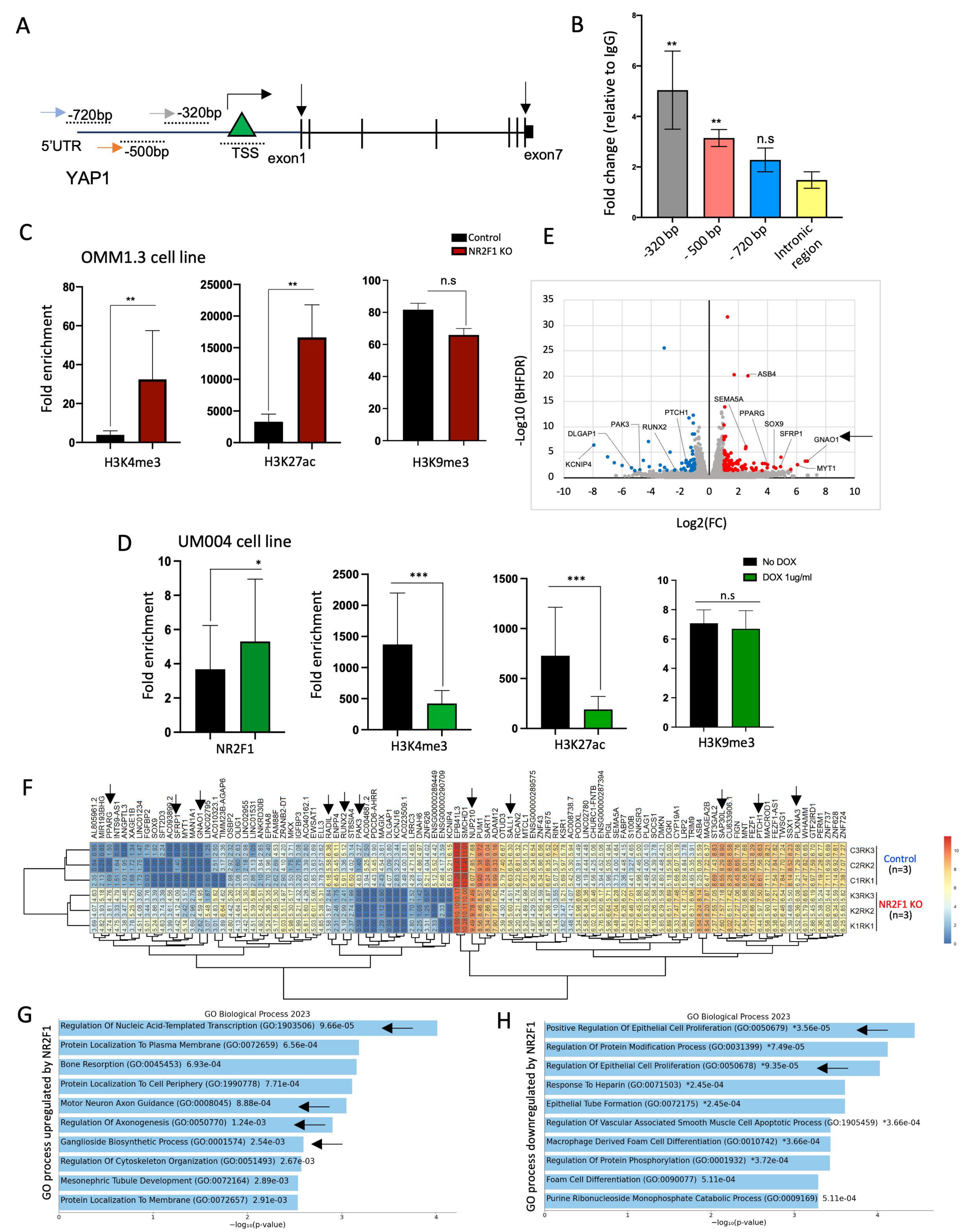
A
-720bp
-320bp
5'UTR
-500bp
TSS
exon1
exon7
YAP1
B
Fold change (relative to IgG)
**
**
n.s
-320 bp
-500 bp
-720 bp
Intronic region
C
OMM1.3 cell line
Control
NR2F1 KO
Fold enrichment
**
**
n.s
H3K4me3
H3K27ac
H3K9me3
E
-Log10 (BHFDR)
Log2(FC)
ASB4
SEMA5A
PPARG
SOX9
SFRP1
GNAO1
MYT1
PTCH1
PAK3
RUNX2
DLGAP1
KCNIP4
D
UM004 cell line
No DOX
DOX 1ug/ml
Fold enrichment
*
***
***
n.s
NR2F1
H3K4me3
H3K27ac
H3K9me3
F
Control (n=3)
NR2F1 KO (n=3)
C3RK3
C2RK2
C1RK1
K3RK3
K2RK2
K1RK1
G
GO Biological Process 2023
GO process upregulated by NR2F1
Regulation Of Nucleic Acid-Templated Transcription (GO:1903506) 9.66e-05
Protein Localization To Plasma Membrane (GO:0072659) 6.56e-04
Bone Resorption (GO:0045453) 6.93e-04
Protein Localization To Cell Periphery (GO:1990778) 7.71e-04
Motor Neuron Axon Guidance (GO:0008045) 8.88e-04
Regulation Of Axonogenesis (GO:0050770) 1.24e-03
Ganglioside Biosynthetic Process (GO:0001574) 2.54e-03
Regulation Of Cytoskeleton Organization (GO:0051493) 2.67e-03
Mesonephric Tubule Development (GO:0072164) 2.89e-03
Protein Localization To Membrane (GO:0072657) 2.91e-03
−log10(p-value)
H
GO Biological Process 2023
GO process downregulated by NR2F1
Positive Regulation Of Epithelial Cell Proliferation (GO:0050679) *3.56e-05
Regulation Of Protein Modification Process (GO:0031399) *7.49e-05
Regulation Of Epithelial Cell Proliferation (GO:0050678) *9.35e-05
Response To Heparin (GO:0071503) *2.45e-04
Epithelial Tube Formation (GO:0072175) *2.45e-04
Regulation Of Vascular Associated Smooth Muscle Cell Apoptotic Process (GO:1905459) *3.66e-04
Macrophage Derived Foam Cell Differentiation (GO:0010742) *3.66e-04
Regulation Of Protein Phosphorylation (GO:0001932) *3.72e-04
Foam Cell Differentiation (GO:0090077) 5.11e-04
Purine Ribonucleoside Monophosphate Catabolic Process (GO:0009169) 5.11e-04
−log10(p-value)

A

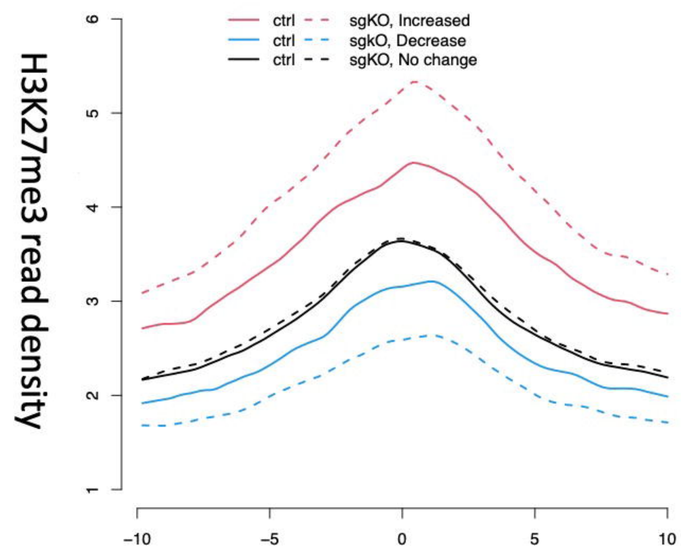
ctrl sgKO, Increased
ctrl sgkO, Decrease
ctrl sgKO, No change
H3K27me3 read density
Distance to peak center
(x10 kb)

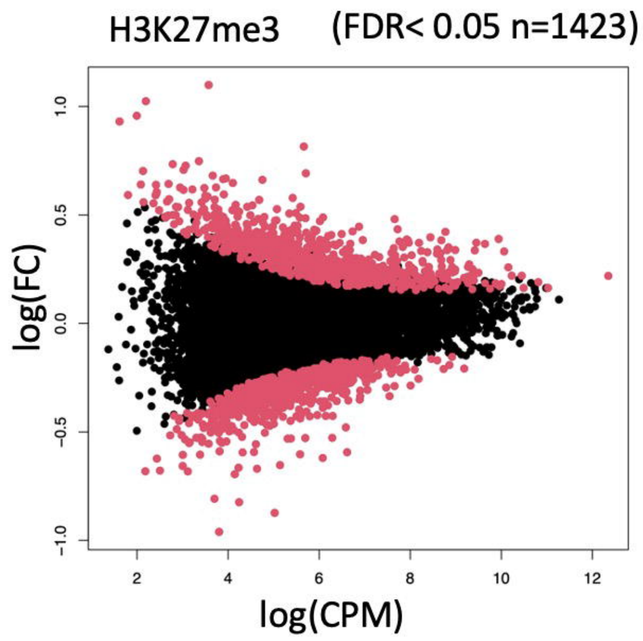
H3K27me3 (FDR< 0.05 n=1423)
log(FC)
log(CPM)

B

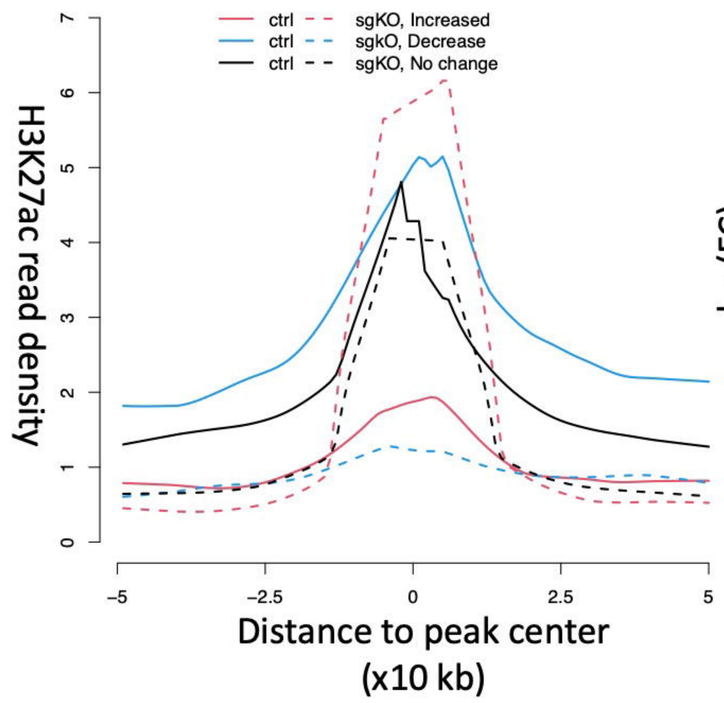
ctrl sgKO, Increased
ctrl sgkO, Decrease
ctrl sgKO, No change
H3K27ac read density
Distance to peak center
(x10 kb)

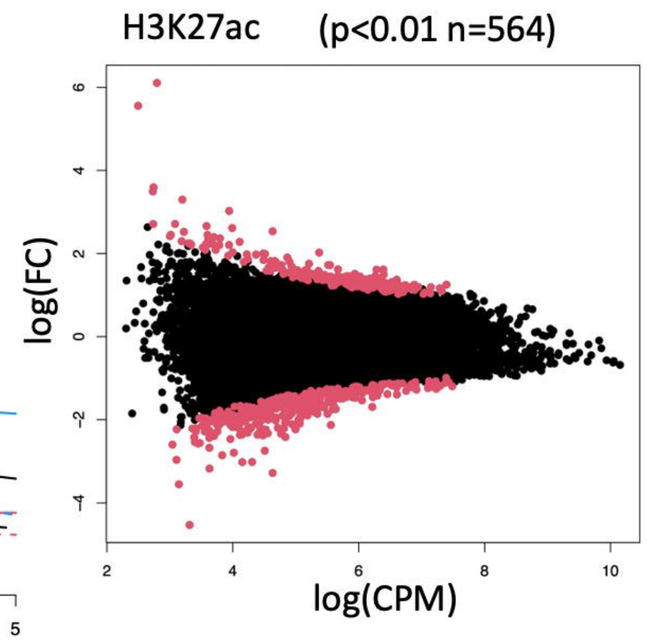
H3K27ac (p<0.01 n=564)
log(FC)
log(CPM)

C

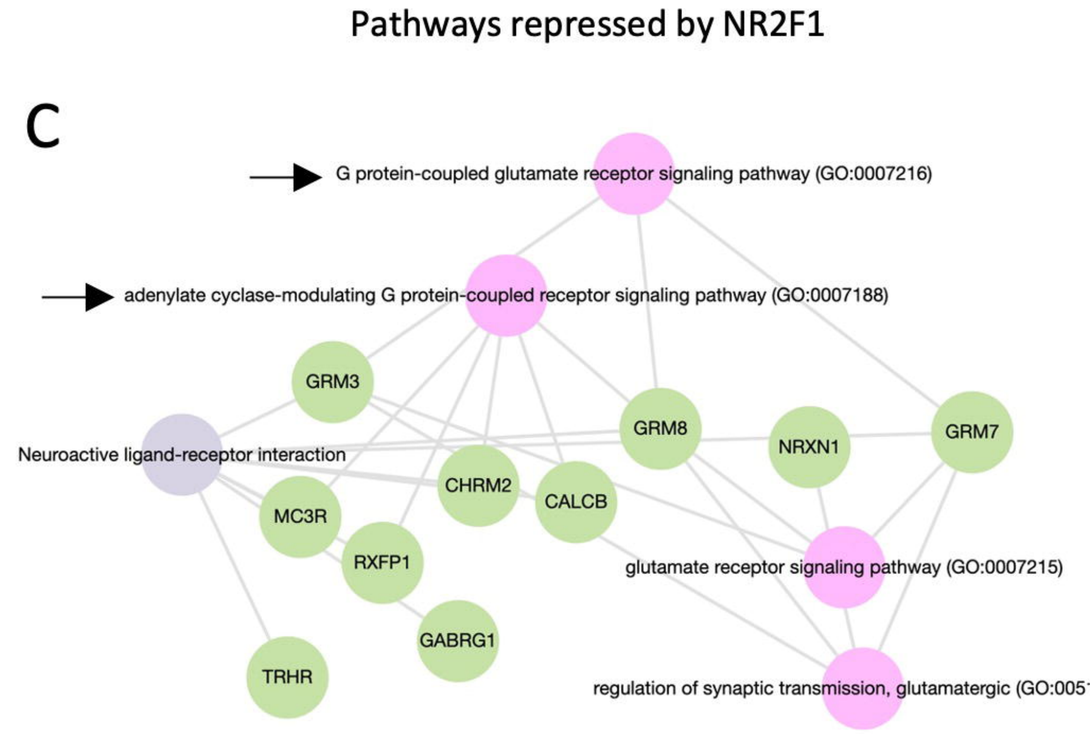
Pathways repressed by NR2F1
G protein-coupled glutamate receptor signaling pathway (GO:0007216)
adenylate cyclase-modulating G protein-coupled receptor signaling pathway (GO:0007188)
Neuroactive ligand-receptor interaction
GRM3
GRM8
NRXN1
GRM7
CHRM2
CALCB
MC3R
RXFP1
GABRG1
TRHR
glutamate receptor signaling pathway (GO:0007215)
regulation of synaptic transmission, glutamatergic (GO:005

D

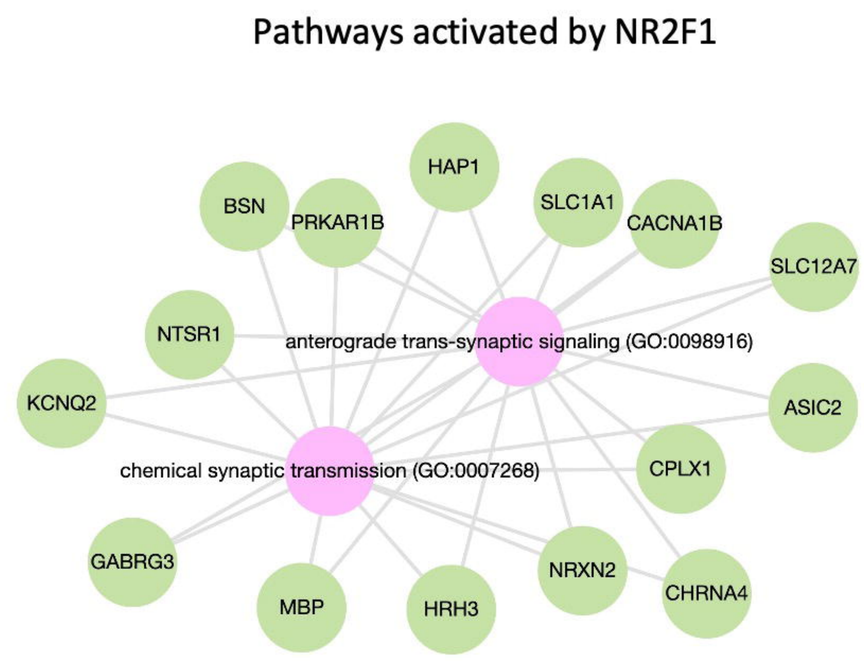
Pathways activated by NR2F1
HAP1
BSN
PRKAR1B
SLC1A1
CACNA1B
SLC12A7
NTSR1
anterograde trans-synaptic signaling (GO:0098916)
KCNQ2
ASIC2
chemical synaptic transmission (GO:0007268)
CPLX1
GABRG3
NRXN2
CHRNA4
MBP
HRH3

E

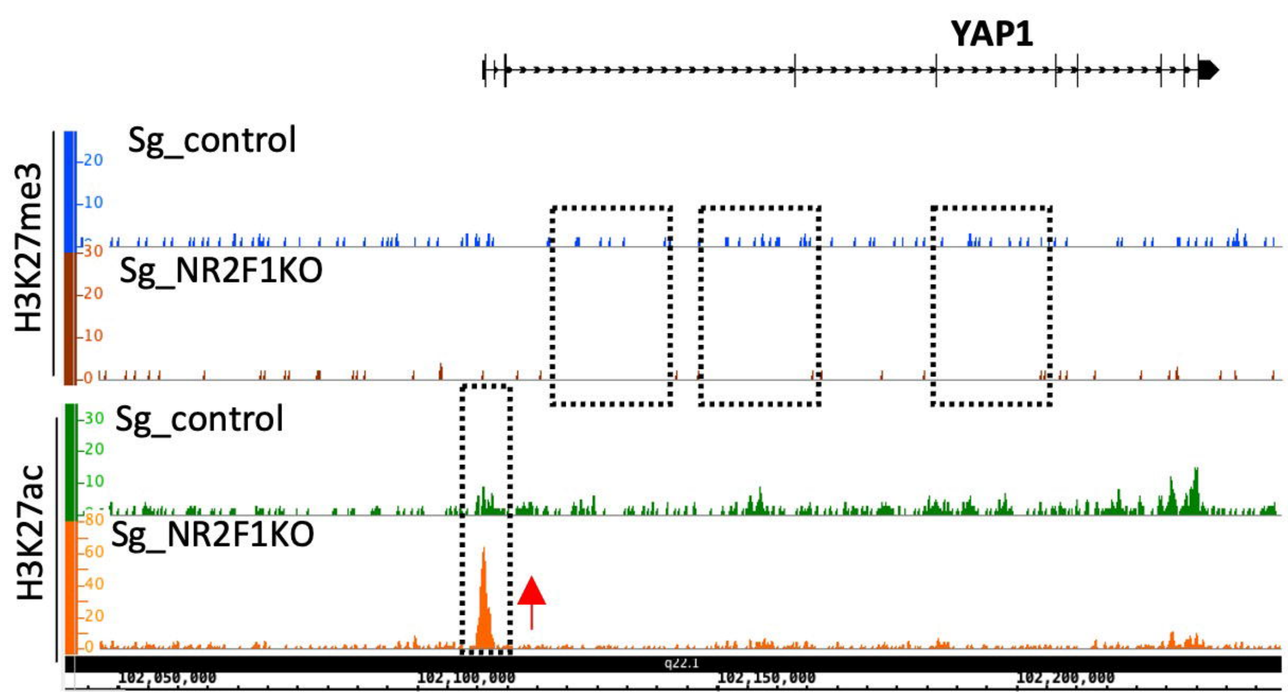
YAP1
Sg_control
Sg_NR2F1KO
H3K27me3
Sg_control
Sg_NR2F1KO
H3K27ac

F

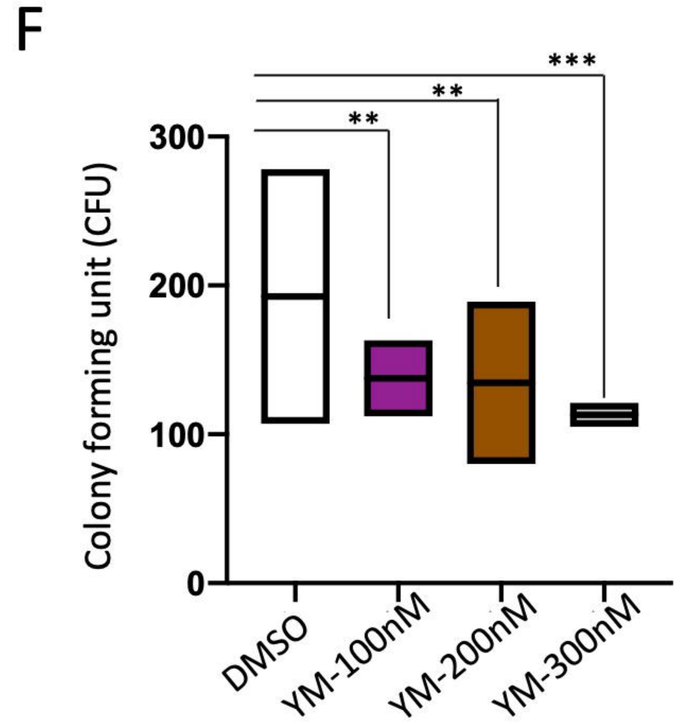
Colony forming unit (CFU)
DMSO
YM-100nM
YM-200nM
YM-300nM

G

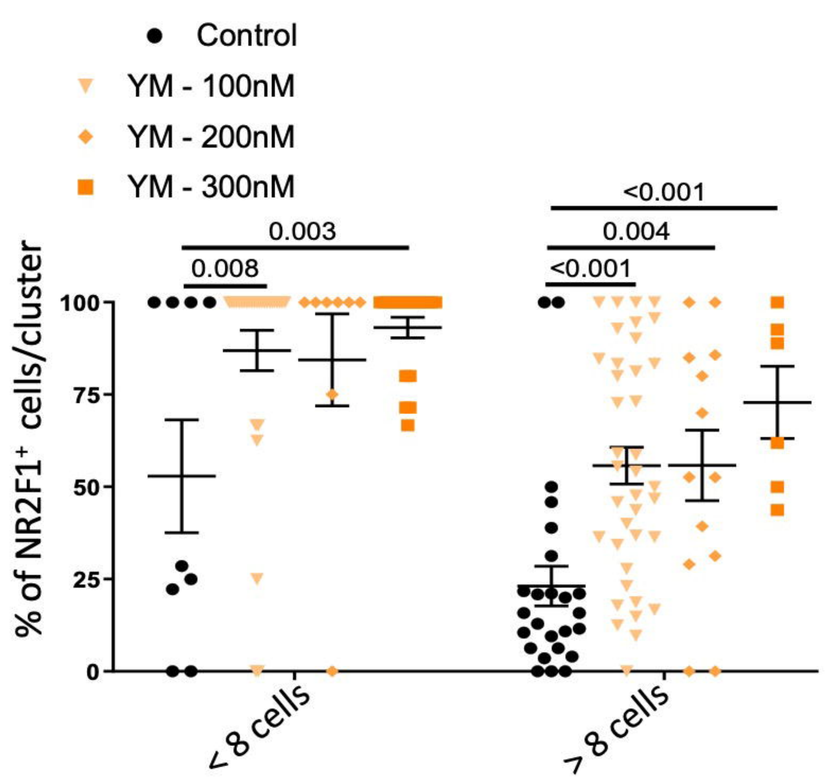
Control
YM - 100nM
YM - 200nM
YM - 300nM
% of NR2F1+ cells/cluster
< 8 cells
> 8 cells

H

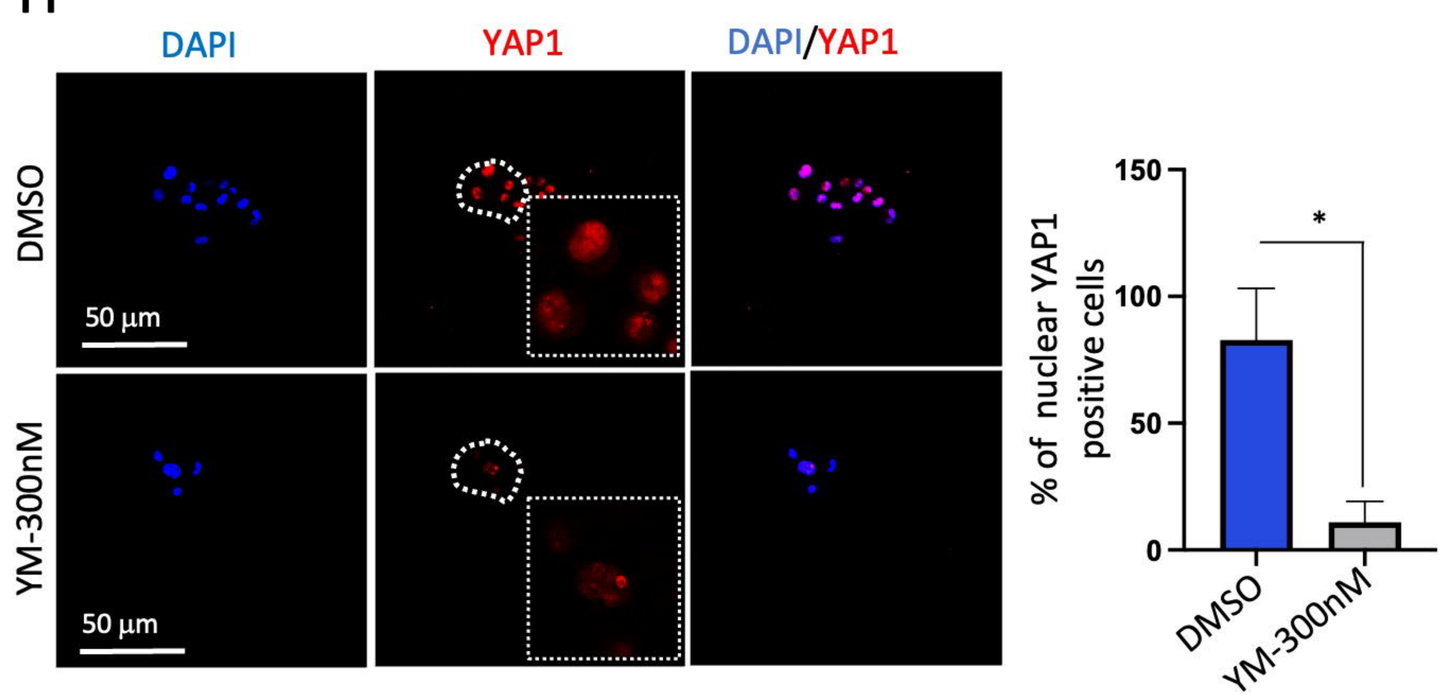
DAPI
YAP1
DAPI/YAP1
DMSO
YM-300nM
50 µm
% of nuclear YAP1 positive cells
DMSO
YM-300nM

Graphical abstract

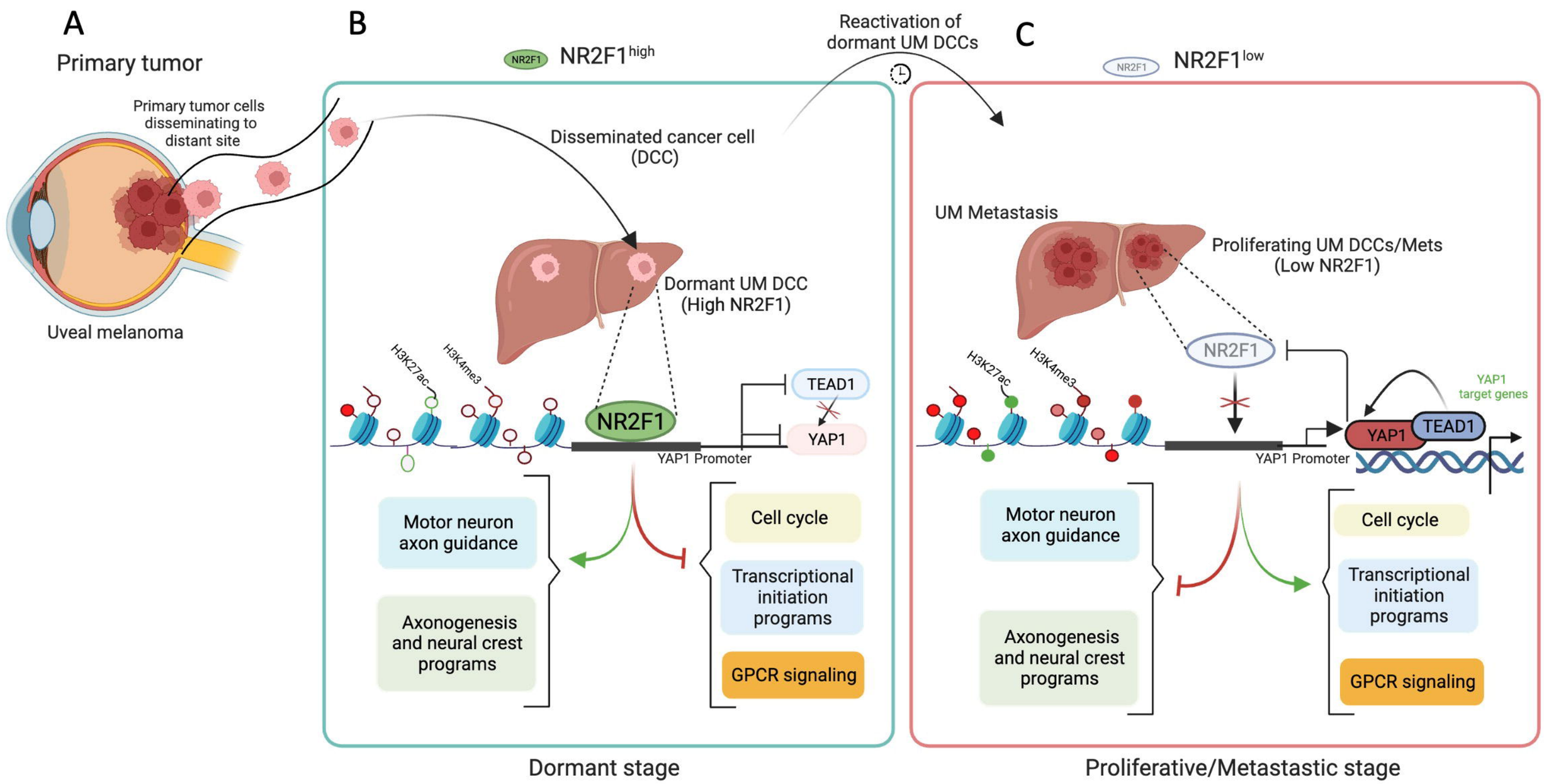

UM cells disseminate to the liver and stay dormant for a prolonged period before manifesting as overt metastasis(A). Dormant UM DCCs express high levels of NR2F1 which induces transcriptional repression of YAP1 by binding to its promoter (B). Binding of NR2F1 inhibits recruitment of H3K4me3 and H3K27ac gene activation marks onto YAP1 promoter and globally represses programs related to cell cycle proliferation, transcriptional initiation and GPCR signaling while activating axonal guidance and neural crest migration pathways in dormant UM DCCs (B). With time, dormant UM DCCs lose NR2F1 expression (C) and are reawakened to give rise to overt metastasis as NR2F1 binding onto the YAP promoter is reduced leading to activation of YAP1 oncogenic signaling (C). Also, YAP1 inhibits NR2F1 expression through unknown mechanisms causing activation of cell cycle proliferation, transcriptional initiation and GPCR pathways and inhibition of neuronal programs (C).